Journal of Quaternary Science

ICE MARGIN OSCILLATIONS DURING DEGLACIATION OF THE NORTHERN IRISH SEA BASIN

Journal:	*Journal of Quaternary Science*
Manuscript ID	JQS-18-0014
Wiley - Manuscript type:	Research Article
Date Submitted by the Author:	04-Feb-2018
Complete List of Authors:	Chiverrell, Richard; University of Liverpool, Department of Geography Smedley, Rachel ; University of Liverpool, Department of Geography and Planning Small, David; Durham University, Department of Geography Ballantyne, Colin; University of St Andrews, Geography and Geoscences Burke, Matthew; University of Liverpool, Department of Geography and Planning Callard, Louise; Durham University, Department of Geography Clark, Chris; Univ Sheffield, Dept Geography Duller, Geoffrey; Aberystwyth University, Department of Geography and Earth Sciences Evans, David; Durham University, Geography Fabel, Derek; Scottish Universities Environmental Research Centre van Landeghem, Katrien; Bangor University, School of Ocean Sciences Livingstone, Stephen; University of Sheffield, Geography Ó Cofaigh, Colm; Durham University, Department of Geography Thomas, Geoff; University of Liverpool, Geography; Roberts, David; Durham University, Geography Saher, Margot; Bangor University, School of Ocean Sciences Scourse, James; University of Exeter College of Life and Environmental Sciences Wilson, Peter; University of Ulster, School of Environmental Sciences
Keywords:	British-Irish Ice Sheet, Irish Sea Ice Stream, Heinrich Event 1, luminescence dating, cosmogenic nuclide dating

ICE MARGIN OSCILLATIONS DURING DEGLACIATION OF THE NORTHERN IRISH SEA BASIN

R.C. Chiverrell[1*], R.K. Smedley[1,2,3], D. Small[4], C.K. Ballantyne[5], M.J. Burke[1], S.L. Callard[6], C.D. Clark[7], G.A.T. Duller[2], D.J.A. Evans[6], D. Fabel[8], K. van Landeghem[9], S. Livingstone[7], Ó Cofaigh, C.[6], G.S.P. Thomas[1]. D.H. Roberts[6], M Saher[9], J.D. Scourse[10], P. Wilson[11]

[1]School of Environmental Sciences, University of Liverpool, Liverpool, UK

[2]Department of Geography and Earth Sciences, Aberystwyth University, Ceredigion, UK

[3]School of Geography, Geology and the Environment, Keele University, Keele, Staffordshire, UK

[4]School of Geographical and Earth Sciences, University of Glasgow, Glasgow, UK

[5]School of Geography and Sustainable Development, University of St Andrews, St Andrews, UK

[6]Department of Geography, Durham University, Durham, UK

[7]Department of Geography, University of Sheffield, Sheffield, UK

[8]Scottish Universities Environmental Research Centre, East Kilbride, UK

[9]School of Ocean Sciences, Bangor University, Menai Bridge, Anglesey, UK

10College of Life and Environmental Science, University of Exeter, Cornwall, UK

[11]School of Geography and Environmental Sciences, University of Ulster, Belfast, UK

(*E-mail: RCHIV@LIV.AC.UK)

ABSTRACT

We present a new chronology to constrain ice-margin retreat in the northern Irish Sea Basin. Estimates on the timing of ice thinning derived from CN ages for boulders from the summits of the Isle of Man and southwest Cumbria suggest that ice thinning was commensurate with the rapid retreat that followed the short-lived advance of the Irish Sea Ice Stream (ISIS) to maximum limits in the Celtic Sea. This ice retreat in the northern ISB was fastest at 20 ka in response to a wider calving margin, but slowed as ice stabilised and oscillated against the Isle of Man. We provide the first age constraints for the Scottish Readvance (19.2-18.2 ka) and demonstrate that it was potentially regional event across the Isle of Man and Cumbrian lowlands not linked with Heinrich event 1. After the Scottish Readvance ca. 19 ka, the ice front retreated northwards towards the Southern Uplands at the same time as climate north of ~45 °N warmed in response to summer insolation. This sequence demonstrates the importance of internal dynamics in controlling ice retreat rates in the Irish Sea, but also that deglaciation of the northern ISB was a response to climate warming.

KEYWORDS: British-Irish Ice Sheet; Irish Sea Ice Stream; Heinrich Event 1; luminescence dating; cosmogenic nuclide dating.

PAPER: 8700 WORDS

1. INTRODUCTION

During the Last Glaciation (Marine Isotope Stage 2), ice flowed westwards into the northern Irish Sea Basin (NISB) from Ireland, SW Scotland and the English Lake District (Fig. 1). From the subglacial bedform record in the NISB and surrounding areas, Livingstone et al. (2012) identified flowsets that represent three phases of ice movement. The earliest (Phase I) flow of ice from southwest Scotland and the Lake District extended both southwards across the NISB eastwards through the Tyne and Stainmore Gaps. The extensive subglacial bedforms of Phase II indicate northeastwards migration of an ice divide across the Carlisle lowlands, and the development of convergent ice flows west and southwest into the NISB during draw-down of the Irish Sea Ice Stream (ISIS) (Livingstone et al., 2012). This pattern conforms with evidence on the Isle of Man (Roberts et al., 2007) and central Irish Sea (Van Landeghem et al., 2009). The bedforms attributed to Phase III indicate that unconfined southerly flow of ice from SW Scotland reached the Carlisle lowlands and deposited ice-marginal landforms (Livingstone et al., 2010c) that have been attributed to the Scottish Readvance originally proposed by (Trotter and Hollingworth, 1932; Trotter et al., 1937).

The NISB is bathymetrically asymmetric, reaching depths of - 45 m in the west but shallowing to -40 m in the east (Fig. 1). In the Solway Firth, a west-east aligned basin descends gradually over ~100 km to a depth of -65 m, then steeply to -145 m in western part of the main basin. Global isostatic modelling (GIA) by Bradley et al. (2011) suggests that between 24 ka and 16 ka relative sea levels were ~30 m below present, implying that the ISIS had a marine-terminating margin in the western part of the NISB, but was at least partly grounded in the eastern part. Smedley et al. (2017b) have shown that retreat of the ISIS margin from the southern Irish Sea Basin was complete by 20.3 ± 0.6 ka; it follows that deglaciation of the NISB coincided with summer insolation-related warming at ~45°N (Bintanja et al., 2005) and overlapped the timing of peaks in ice-rafted debris flux to the southern Celtic Sea associated with Heinrich event 1 (Haapaniemi et al., 2010).

The NISB was subjected to multiple standstills or minor (0.1 - 1 km) readvances of the ice margin during deglaciation of differing palaeoclimatic significance (e.g. Thomas et al., 2004). This deglacial signature is recorded in extensive seafloor sediments (Pantin et al., 1978) and in adjacent terrestrial sediments and landforms (Livingstone et al., 2008, 2010a; Livingstone et al., 2010c; Livingstone et al., 2012; McCabe, 2008; Merritt and Auton, 2000; Thomas, 1977; Thomas et al., 2004). The eastern and western Irish Sea mud belts (Jackson et al., 1995; Pantin et al., 1978) are basins filled with substantial thicknesses (>10 m) of Holocene sediment and bury the glacial stratigraphy. The Holocene sediment fill in the Solway Firth is thinner, and there is a greater potential for the visibility of glacigenic landforms on the sea floor (Jackson et al., 1995; Pantin et

al., 1978). The morpho-stratigraphical evidence for movements of the ice margins includes multiple advance-retreat cycles on the Isle of Man (Thomas, 1977, 1984; Thomas et al., 2004; Thomas et al., 2006), and the Gosforth and Scottish readvances in northwest England (Huddart, 1971, 1977; Huddart and Glasser, 2002; Livingstone et al., 2008; Livingstone et al., 2010b; Livingstone et al., 2010c; Livingstone et al., 2012; Merritt and Auton, 2000), but they have not been securely dated. Radiocarbon dating of marine microfauna indicates an oscillatory ice-margin retreat into northeast Ireland between 20.5 ka BP and 16.5 ka BP, approximately coeval with the timing of H1 (McCabe, 2008; McCabe et al., 2007; McCabe et al., 1998). Attempts to correlate readvances across the NISB are hampered by limited dating of events in NW England and on the Isle of Man. Here we provide new geochronological, geophysical and stratigraphical data for the rates and style of deglaciation in the ISB, including new multiple surveys of the seafloor, eleven optically stimulated luminescence (OSL) ages, and eight cosmogenic nuclide (CN) ages.

This paper: (1) outlines the nature of the glacial sediment/landform imprint relating the retreat and oscillation of the ISIS; (2) provides chronology to test the existing interpretations that multiple readvances occurred in the NISB during the last deglaciation; (3) assesses the interaction between multiple and disparate ice lobes as these ice margins stepped back; (4) explores the synchrony between marine and terrestrial sectors of the ice mass; and (5) considers the forcing factors controlling ice retreat and readvances.

2. METHODS

2.1 Terrestrial sites and sampling

The style and timing of deglaciation in the NISB has been discerned from terrestrial evidence for changes in geomorphology, the sediment-landform assemblages and interpreted patterns of ice flow (Livingstone et al., 2008, 2010a; Livingstone et al., 2012; McCabe, 2008; Merritt and Auton, 2000; Roberts et al., 2007; Thomas, 1977; Thomas et al., 2006). The ice retreat model is conceptualised here in terms of seven broad zones, with seven boundaries (Fig. 1). Eleven samples for OSL dating from eight sites were targeted at glaciofluvial and deltaic outwash sands associated with well-defined terrestrial ice-marginal positions. CN dating using in-situ ^{10}Be targeted both glacially-modified bedrock and glacially-faceted and transported boulders in order to provide eight samples from three locations (Fig. 1). A further eight published CN ages (Ballantyne et al., 2013) were recalibrated using locally-derived ^{10}Be production rates (Fabel et al., 2012). Exposures of the glacial sediments were investigated at coastal sections (Aber Ogwen, Orrisdale, Jurby, Dog Mills and Gutterby), and at the Aldoth, Ballahara and Turkeyland quarries (Fig. 1). Exposures were photographed and logged using field sketches, vertical lithofacies logs and photo-montages following standard procedures (Evans and Benn, 2004; Thomas et al., 2004). The information recorded included textural classification, sedimentary structures, sorting and grain size, palaeo-currents and lithofacies classification. For OSL dating, opaque tubes were hammered into

sedimentary sections to prevent exposure to sunlight during sampling. For CN dating, the rock samples were chiselled from the uppermost boulder and bedrock surfaces. Topographic shielding was measured in the field and corrected for using the CRONUS-Earth online calculator (Balco et al., 2008).

2.2 Offshore geomorphology and geophysics

Unlike other sectors of the ISB, there is a scarcity of palaeoenvironmental data for the waters to the north and east of the Isle of Man. Cruise JC106 of the RRS James Cook (July 2014: Fig. 1) addressed this issue by collecting 380 km of geophysical data and eight cores using the British Geological Survey 6 m vibrocorer and surveying across the seafloor extension of the Bride moraine, east of the Isle of Man (Thomas, 1984). Surveys also extended into the eastern Irish Sea mud-belt (Pantin et al., 1978) and into the deeper waters of the Solway Firth to the north of the Isle of Man (Fig. 1). Geophysical data included multibeam imaging of the seafloor using a Kongsberg EM710 70-100 khz frequency system, with the data processed using CARIS HIPS. An acoustic stratigraphy was also obtained using a hull-mounted Kongsberg SBP120 sub-bottom profiler (chirp frequency range of 2.5-6.5 kHz). Two-way travel times in seconds was converted to depth below sea level at the time of surveying using typical values of sound velocity (1500 m·s-1 through the water column and 1600 m·s-1 through soft sediments). The sub-bottom profiler data were displayed in IHS Kingdom as 2D survey lines. The sediment cores were cut into 1 m long sections, split, photographed and logged recording the sediment shear strength in kPa (Torvane), grain size, sedimentary and deformation structures, colour, sorting, bed contacts, clast abundance and shape and macrofaunal content. We identify five acoustic facies assemblages (AFA1-5; Table 1) from the sub-bottom profiler data. Photographs, visual logs and the physical properties from seven vibrocores were used to attribute lithofacies and depositional environments to the acoustic facies (Table 1).

2.3 OSL dating

External beta dose-rates were determined for OSL dating using inductively coupled plasma mass spectrometry (ICP-MS) and inductively coupled plasma atomic emission spectroscopy (ICP-AES), while the external gamma dose-rates were determined using in-situ gamma spectrometry (Table 2). OSL analysis was performed on single grains of quartz. The sample preparation and analysis methods used for OSL dating were identical to those employed by Smedley et al. (2017b). The single-grain D_e values determined for each sample (Fig. 2) are included in the supplementary material (Table S1 - S11). OSL analyses of all samples were performed on grain sizes of 212 - 250 μm, except for sample T3DOGM01 which had a grain size of 150 – 180 μm and so had up to four grains in each hole during single-grain analysis (i.e. microhole analyses). The Finite Mixture Model (FMM) identified four components in the D_e distribution determined for sample T3DOGM01, where the lowest component (0.5 ± 0.2 ka; n = 3 grains) was inconsistent with the geological context of

the sample i.e. a 0 Gy dose population that was rejected by applying the screening criteria. However, there was a population of grains that gave an OSL age of 6.0 ± 1.2 ka (n = 4 grains) that was positioned halfway between the 0 Gy dose population and the dominant population. Such populations have previously been suggested to be phantom dose populations caused by averaging the OSL signal from more than one grain during analysis (Arnold and Roberts, 2009). This was probably the case for sample T3DOGM01 as the D_e distribution was determined using microhole measurements rather than single grains; thus, we provide a maximum OSL age for sample T3DOGM01 using the Central Age Model (CAM; 21.9 ± 1.9 ka; Table 3). D_e values were calculated using the Central Age Model (CAM) for D_e distributions that were symmetrical and therefore homogeneously bleached prior to burial, while the minimum age model (MAM) was used to determine D_e values for D_e distributions that were asymmetrically distributed and therefore heterogeneously bleached prior to burial (Table 3). The overdispersion determined from dose-recovery experiments estimated the scatter caused by intrinsic sources of uncertainty that is beyond measurements uncertainties. Intrinsic overdispersion was added in quadrature to the extrinsic scatter arising from external microdosimetry (~20 %) to determine σ_b for the MAM. The CAM or MAM D_e values were divided by the environmental dose-rates to determine an age for each sample (Table 3).

2.4 CN dating

Eight rock samples were prepared at the University of Glasgow. Quartz was separated from the 250 – 500 µm fraction using standard mineral separation techniques (c.f. Kohl and Nishiizumi, 1992) and purified by ultrasonication in 2 % HF/HNO_3 to remove remaining contaminants and meteoric ^{10}Be. Be extraction was carried out at the Cosmogenic Isotope Analysis Facility - Scottish Universities Environmental Research Centre (CIAF - SUERC), using procedures based on Child et al. (2000). The ^{10}Be/^{9}Be ratios were measured by accelerator mass spectrometry (AMS) at SUERC (Xu et al., 2010) (Table 4). Eight previously published CN ages determined for boulders from Glen Trool (McCarroll et al., 2010) and Gladbach Brae (Ballantyne et al., 2013) in the Galloway Hills of SW Scotland were recalibrated here (Table 5). All new and existing CN ages were calculated using CRONUS-Earth v2.3 (Balco et al., 2008), applying a local production rate, the Loch Lomond production rate (LLPR) of Fabel et al. (2012), time-dependent Lm scaling (Lal, 1991; Stone, 2000) and an erosion rate of 1 mm ka^{-1}.

2.5 Bayesian age-sequence modelling

The geochronological measurements (Table 6) were interrogated using a Bayesian temporal model (Bronk Ramsey, 2009a). The morpho-stratigraphical model for deglaciation of the NISB (sensu Chiverrell et al., 2013) provided the prior model (i.e. hypothetical 'relative-order' of events), which was developed independently of the age information and conceptually underpinned the Bayesian age modelling (Bronk Ramsey, 2009a, b; Buck et al., 1996). The prior model here is

complex and integrates the relative distance reconstruction of ice-marginal retreat south to north across the Isle of Man and Cumbria, and into the mountain hinterlands of the Lake District and Southern Scotland. The CN ages determined for boulders from South Barrule (Isle of Man) and Black Combe (northwest England) represent the timing of ice thinning rather than ice margin retreat, and so were run as outliers (100%) in the Bayesian model to understand their relationship to ice thicknesses and surface lowering. Note that ages defined as 100 % outliers in a Bayesian Sequence model will not influence the modelled outputs. Bayesian modelling was completed using OxCal 4.2 (Bronk Ramsey and Lee, 2013) and comprised a uniform phase sequence model punctuated by boundaries (see supplemental information). The approach uses Markov chain Monte Carlo (MCMC) sampling to build up a distribution of possible solutions, generating a probability called a posterior density estimate, which is the product of both the prior model and likelihood probabilities for each sample. The approach generated modelled ages for boundaries between seven ice retreat zones (Zone 1 – 7: Fig. 1). Each retreat zone was coded as a Phase and grouped dating information for sites that share a common relationship with other items in the model. Phases were separated by the Boundary command which delimited each Phase and generated the modelled output of ages (referred to as BL1 to 7: Fig. 1). The Sequence model was run in an outlier mode to assess outliers in time using a student's t-distribution ($p < 0.2$) to describe the distribution of outlier and an outlier scaling of 10^0 – 10^4 years (Bronk Ramsey, 2009b).

3. RESULTS

3.1 Coastal lowlands of North Wales (Zone 1)

Zone 1 describes the step back of ice margins from Anglesey and the Arfon lowlands towards the southern tip of the Isle of Man (Fig. 1). Bedforms from the seafloor between Anglesey and the Isle of Man show east-northeast to west-southwest ice flow directions (Van Landeghem et al., 2009), which suggest an ice margin configuration aligned broadly north-south, and an ice-marginal retreat direction to the northeast. At Aber Ogwen (Edge et al., 1990), coastal exposures show a basal glacial diamict of Welsh provenance overlain by a 2 m thick sequence of laminated sands, silts and clays off-lapping west to east from a diamict high. This lacustrine and deltaic ice-marginal sequence is capped by glacial diamict of Irish Sea affinity. Smedley et al. (2017a) dated two OSL samples which targeted a 0.15 m thick unit of horizontally stratified medium to coarse sand (Sh) above the basal diamict (T4ABER01; 18.1 ± 1.6 ka) and a 0.06 m thick unit of horizontally stratified medium-to-coarse ice proximal bottom-set sands (T4ABER03; 20.1 ± 0.7 ka). These glacigenic sediments on the north Wales coast constrain the unzipping of Irish Sea ice from the Welsh Mountains (BL1: Fig. 1).

3.2 The south of the Isle of Man (Zone 2)

The Plain of Malew (Fig. 3; Roberts et al., 2007; Thomas et al., 2006) records the initial step-back of ice margins in the south of the Isle of Man. River channel diversions suggest that coastal areas were occupied by ice longer than the adjacent Southern Manx Uplands. This suggests ice thinning on the Isle of Man, but the lack of landforms related to ice-marginal positions and dead ice suggests rapid deglaciation rather than in-situ, ablation-driven downwasting (Roberts et al., 2007). Two CN samples were taken from the upper surface of a roche moutonnée (mid-stoss position), which targeted quartz-rich sandstone (T3CREG01) and a quartz vein in the sandstone (T3CREG02) at ~133 m OD on the Cregneash Peninsula, southwest Isle of Man. The striae in this ice moulded terrain indicate overriding by ice flowing NNW-SSE over the peninsula (Lamplugh, 1903). The CN ages determined for T3CREG01 (21.2 ± 1.2 ka) and T3CREG02 (20.9 ± 1.1 ka) are consistent. The low-lying (< 10 m OD) Plain of Malew comprises undulating terrain (< 20 m OD) comprising drumlins in the east, with deglacial outwash sand and gravel plains to the south (Lamplugh, 1898; Lamplugh, 1903; Roberts et al., 2007; Thomas et al., 2004; Thomas et al., 2006). Exposures of these outwash deposits reveal a thin sequence (~2 m) of sand and gravel overlying the limestone on the southeast coast (Fig. 3), where a flat-topped outwash terrace yielded horizontally-stratified coarse sands (Sh) with some granular gravel for OSL dating (T3TURK01), which overlies a unit of pebble gravels. The single-grain D_e distribution determined for T3TURK01 was symmetrical (Fig. 2a) and therefore was expected to have been well bleached prior to burial. T3TURK01 was taken from a thin sequence of glacial outwash sand and gravel and therefore probably was deposited in an environment with greater opportunity for sunlight bleaching prior to burial due to transportation in a shallow water column. The CAM age determined for T3TURK01 (19.2 ± 2.0 ka) is consistent with the CN ages determined from Cregneash, and together they constrain the retreat of ice from the south of the Isle of Man (BL2: Fig. 1).

CN samples were taken at higher altitudes on South Barrule, the highest peak (483 m) in the Manx Southern Uplands and targeted a train of granite erratic boulders (Darwin, 1848). These erratics were transported ~200 m uphill by ice from bedrock exposures at the head of the Foxdale valley. Sample T3BARR01 was taken from a large (2 x 1.5 x 1 m) rounded quartz-rich granite boulder at 467 m near the summit of South Barrule with an exposure age of 25.0 ± 1.4 ka (Fig. 4a). Sample T3BARR02 was taken from a smaller (1 x 1 x 1 m) rounded quartz-rich granite boulder at 390 m produced an exposure age of 18.9 ± 1.0 ka (Fig. 4b). These boulders cannot be linked to specific configurations of the former ice margins, but do potentially constrain the timing of ice sheet thinning in the centre of the ISB.

3.3 Central Valley of the Isle of Man (Zone 3)

The Peel Embayment is located at the western end of the fault-bounded Central Valley of the Isle of Man and contains a complex geomorphology (Fig. 5a) that developed at the lateral margins of

western Irish Sea ice (Thomas et al., 2006). Moraine ridges and confined sandar arc south and southwest, and record ice penetration from the west coast of the Isle of Man (Fig. 5a). A small lake (~10 km^2) trapped between the ice margin and the watershed of the Central Valley (at ~50 m OD) facilitated the development of an ice-contact delta. Quarry exposures in this delta at Ballaharra (Fig. 5b) display a sedimentary sequence of ice proximal deltaic sands and gravels (Gt and St), which dip broadly southeast with an ice contact slope immediately to the north (maximum elevation ~50 m). The uppermost 2 m are planar cross-stratified sands and gravels reflecting a weakly developed delta top-set. Sample T3BALH01 (Fig. 5d) was taken low in the sequence from fine to medium sands (St and Sh) with fine laminations (Fl), which are representative of lower flow conditions in delta toe-sets. Sample T3BALH02 (Fig 5c), from higher in the sequence, was taken from medium to coarse sands (Sr) within planar cross-stratified back-bar gravels (Gp), probably also deposited during declining river flows on the delta top-set. These OSL ages are age-inverted with the upper sample being older (T3BALH02; 27.1 ± 3.8 ka) than the lower (T3BALH01; 18.5 ± 3.3 ka). The single-grain D_e distributions for the two samples suggest that the minimum dose population was characterised better for T3BALH01 (Fig. 2b, 2c). This probably accounts for the age inversion, with T3BALH02 overestimating the true burial age by constraining poorly the well bleached part of a partially-bleached D_e distribution. The coarser-grained T3BALH02 (Sr, Gp) was deposited in a more energetic setting, potentially with less opportunity for bleaching than the finer-grained suspension rain-out deposits T3BALH01 (St, Sh, Fl). Thus, the OSL age for T3BALH01 constrains the timing of this ice margin (BL3: Fig. 1) and the establishment of an ice dammed lake in the Central Valley (Fig. 5).

3.4 Orrisdale ice marginal oscillations (Zone 4)

The Orrisdale formation is one of three major glacigenic formations exposed on the northern coastal plain of the Isle of Man (Fig. 6) (Chadwick et al., 2001; Thomas et al., 2004). The terrain comprises a series of moraine ridges, moraine-confined sandar and lake basins on the northwest coast. Thomas et al. (1985) divided the thick accumulations of glaciofluvial outwash deposits (Bishop's Court Member) into: (i) a coarser gravel-dominated ice proximal lithofacies assemblage (LFA1); and (ii) a finer sand-dominated ice distal lithofacies assemblage (LFA2). Diamict ridges exposed in coastal cliff sections (Fig. 6; Orrisdale Head Member) separated the sandar deposits into six adjacent, ice-marginal and parallel troughs. These record ice retreat northwards when the Irish Sea ice pulled back from the bedrock core of the Isle of Man. The northernmost sandar trough at Orrisdale comprises a stratigraphically younger sequence (trough 6) of distal sandar deposits (LFA2) and was sampled for OSL dating (T3ORIS01) (Fig. 7A). Off-lapping this ridge structure are deposits of medium-to-fine sands (Sp and Sh) with ripples (Sr) and fine laminations (Fl) of LFA2. Sample T3ORIS01 was taken from Sr lithofacies within the back-bar deposits of planar cross-stratified sands (Sp). Although the central value of the OSL age for Orrisdale (T3ORIS01; 23.8 ± 3.1 ka) is older than the constraining OSL ages for Ballaharra and Jurby, it lies within uncertainties

of these OSL ages and the minimum dose population in the single-grain D_e distribution appears to be well characterised due to the large number of D_e values determined for this sample (n = 79 grains; Fig. 2d); thus, it is considered accurate. On the east coast of the northern plain, subglacial diamictons associated with the Orrisdale Formation are restricted to three off-lapping sequences entirely to the north of the Bride Moraine (Thomas et al., 2004). South the Bride Moraine, the Dog Mills member consists of laminated, occasionally massive, fine and silty sands deposited in a proglacial lagoon of lacustrine to shallow marine nature (Thomas et al., 2004). These horizontally-bedded fine to medium sands (Sh) were sampled for OSL dating (T3DOGM01) (Fig. 6 and 7C). The sampled section was capped by a variable sequence of massive and bedded diamicts (supraglacial massive diamictons), which were intercalated and overlain by sands and gravels (the Kionlough Member) that thin southwards from the Bride Moraine (Thomas et al., 2004). The OSL age for T3DOGM01 could only provide a maximum age for deglaciation at Dog Mills (<22.5 ± 2.2 ka) due to the previously discussed presence of phantom dose populations. However, it was consistent with the overall ice-retreat sequence. The Zone 4 ice margin crosses the Isle of Man and extends east towards England, and together the OSL ages from Orrisdale and Dog Mills constrain the timing of ice retreat from BL4 (Fig. 1).

3.5 Southwest Cumbria and northern-most Isle of Man (Zones 5 and 6)

Terrestrial geomorphological data indicate more substantial ice marginal readvances late during the deglaciation of the NISB. Prominent amongst these is the Scottish Readvance, which potentially involved >10 km of ice margin retreat and readvance, in northern England (Livingstone et al., 2010c; Merritt and Auton, 2000) and a series of readvances in northeast Ireland, in part linked with H1 (McCabe et al., 1998). The Scottish Readvance ice margin is postulated to have extended across the lowlands of Cumbria (Fig. 1) and into the eastern ISB down the coast of Cumbria (Livingstone et al., 2010c; Merritt and Auton, 2000; Trotter et al., 1937). It has also been linked (Livingstone et al., 2010c) with a series of readvances north of the Bride Moraine on the Isle of Man (Thomas et al., 2004). The thin geometry of the associated till in the Solway Lowlands (Livingstone et al., 2010d; Trotter and Hollingworth, 1932) and the glaciotectonised succession within the St Bees and Gutterby moraines (Williams et al., 2001) led to suggestions that the Scottish Readvance was a short-lived event. The flow phases and ice-marginal positions are currently based on stratigraphy, rather than geochronological information. Connection of these ice margins across the northeast ISB is uncertain, and so the structure and timing of this readvance episode has yet to be resolved fully. Here we address this with a new geochronology for ice-marginal advances within the Jurby Formation on the Isle of Man (Thomas et al., 2004), the Gutterby coastal sections in the southwest Lake District (Huddart, 1977, 1991) and for the Holme St Cuthbert delta complex in lowland Cumbria (Livingstone et al., 2010c).

Jurby, northern Isle of Man: The coastal sections at Jurby on the west coast of the Isle of Man were deposited during a phased 2 – 3 km readvance of the ISIS ice margin into a subaqueous fronting basin (Thomas et al., 2004). The stratigraphy shows four similar off-lapping sediment packages that contain ice contact diamict and subaqueous fan sand-to-mud, grading to distal, laminated muds (Fig. 7B) (Thomas et al., 2004). The Jurby Formation represents a series of readvances of relatively thin ice that extended ~400 – 500 m further than the previous advance, and unconformably overlies the diamictons of the Orrisdale Formation. These advances were followed by rapid retreat during which there was limited erosion or burial of the sediment succession. OSL sampling targeted the second of these sediment packages. The basal sediments are composed of diamict (Orrisdale Head Member) that is unconformably overlain by sands and the massive muds of the Jurby Formation (Thomas et al., 2004). This sequence was then capped by a late glacial kettle hole infill (Fig. 7B). The sampled sands are interpreted as low-energy outwash from subglacial channels evacuating water and sediment either directly or via a short subaerial sandur into open water. OSL samples were taken from a unit of laminated medium to coarse sand (Sh) (T3JURB01) and fine to medium, upward-fining rippled sands (Sh and Sr) (T3JURB02). Both samples were taken from the middle of the cliff section, which is capped by massive muds (Fig. 7B). OSL ages of 20.8 ± 2.4 ka (T3JURB01) and 23.4 ± 2.8 ka (T3JURB02) were determined, but, although these OSL ages overlap within uncertainties, the age for T3JURB02 appears relatively old. This is related potentially to the larger population of D_e values measured for sample T3JURB01 (Fig. 2j; n = 105 grains), which better characterised the minimum dose population in comparison to T3JURB02 (Fig. 2k; n = 83 grains). However, 83 grains is a large number of grains, given ~50 grains is typical per sample (e.g. Rodnight et al., 2006), and therefore suggests that this sample was very poorly bleached. Poor bleaching is consistent with the relatively short transport pathway interpreted for these grains via a subaerial sandur into a water body.

Western Lake District: The coastal plain of southwest Cumbria comprises a low-level <50 m OD undulating terrain of mounds, ridges and basins dissected by outwash channels that formed between the Irish Sea ice mass and Cumbrian Fells (Merritt and Auton, 2000). Samples for CN dating were collected from four glacially-transported boulders of Eskdale granite on the western slopes (255 m OD) of Black Combe (600 m OD), which was approximately 4 km northeast of, and 250 m higher than Gutterby (Fig. 1). The boulders were originally sourced from the southern margin of a granite outcrop located 3 km to the north of Black Combe, and protrude at least 0.75 m in height above the present ground surface and positioned within 150 m of one another (Fig. 4C-F). We infer that the suite of boulders was deposited as the ice was downwasting and retreating. Current water depths in the adjacent ISB suggest that ice thicknesses >300 m were required to deposit the boulders on this lateral margin. This therefore corresponded to the lowering of the ice stream during deglaciation. The four CN samples yielded ages of 16.6 ± 0.9 ka, 24.0 ± 1.2 ka, 21.1 ± 1.1 ka and 22.0 ± 1.2 ka (Table 4), and show significant variation for an individual site. Of these

ages, three (T3BC03, 05 and 06) overlapped within ± 1σ uncertainties, and provided a weighted mean age of 22.3 ± 1.2 ka that represents the best estimate of the timing of ice surface lowering to ~260 m in the eastern Lake District.

The Annaside-Gutterby complex is composed of north-south aligned ice-marginal ridges that have been associated with readvances of Irish Sea ice down the Cumbrian coastline (Fig. 9). These ridges have been linked with both the Scottish and Gosforth readvances (Huddart, 1977, 1991; Merritt and Auton, 2000), but this has not been supported by any robust chronology. Coastal exposures through the ridges of the Annaside-Gutterby complex show a sequence of glacial diamictons, outwash sands and gravels, and glaciolacustrine sediments (Fig. 9). The basal sediments near Annaside Banks are composed of horizontally-stratified, planar cross stratified and rippled sands (Sh; Sp and Sr) with occasional fine drapes (Fl) that were deposited in a shallow lacustrine setting (Huddart, 1991); these sands were sampled for OSL dating (T3GUTT01). Thick sequences of glaciolacustrine silts/clays interbedded with outwash sands bury these basal sands and reflect a readvance of ice. A second coastal section, 1.2 km to the south of T3GUTT01, also shows lower outwash sands overlain by shallow glaciolacustrine silts/clays with occasional dropstones and these are interbedded with glacifluvial rippled and sub-horizontally bedded sands. These sediments are heavily deformed due to soft sediment deformation suggesting rapid accretion but are also cross-cut by sheared and boudinaged zones related to ice readvance and compressive glaciotectonism of the sediment pile. A clear readvance signal is also supported by the coarsening upwards of glaciofluvial sands and gravels and the emplacement of subglacial diamicts into the upper parts of the glacial sequence. The uppermost 5 – 10 m of the cliff section was composed of massive stratified gravels (Gms) and horizontally stratified and ripped sands (Sh and Sr). An OSL sample (T3GUTT03) was taken from the rippled sands between two gravel units in the upper 3.5 m of the sequence. As a pair of samples, T3GUTT01 provides constraint on outwash deposition to 27.0 ± 3.3 ka that predated the readvance responsible for the Annaside-Gutterby ice-marginal, glacitectonised complex and sample T3GUTT03 constrains the ultimate retreat of the ice from this ice-marginal ridge to 21.7 ± 2.6 ka (Fig. 9).

Holme St Cuthbert: The Holme St Cuthbert delta is a 2 km by 4 km lowland (45 m OD) flat-topped ridge composed of sand and gravel, which overlies a predominantly NE-SW aligned drumlinised terrain (Fig 8B) (Livingstone et al., 2008). This superimposition requires that the ice that produced the drumlins must have withdrawn, to be followed by a readvance necessarily from a different direction in order to impound a lake in which the delta could form. The delta developed during a late stage SE readvance of ice into the NISB and provides evidence for a lake in the Solway Lowlands dammed by readvance of ice from SW Scotland (Huddart, 1970; Livingstone et al., 2010c), so a Cumbrian withdrawal and Scottish advance. During December 2013, the quarry sections showed the classic components of an ice contact Gilbert-style delta (Fig. 8A), with three

broad lithofacies assemblages (LFA1-3). LFA1 is a 5 m thick sequence of sub-horizontal sands and granule gravels, typical of delta-proximal toe-sets, in addition to horizontal muds and sands that were deposited as more distal bottom-sets in a low energy environment (Clemmensen and Houmark-Nielsen, 1981; Cohen, 1979; Gustavson et al., 1975; Jopling and Walker, 1968). LFA2 comprises a thick (8 - 9 m) sequence of steeply (30 – 40°) southeast-dipping planar beds of stratified medium-coarse sand with granule to pebble gravels, typical of delta foreset beds deposited as cohesionless subaqueous debris-flows (Nemec, 2009; Nemec et al., 1999; Smith and Ashley, 1985). LFA3 is a ~2 m sequence of glaciofluvial bar-form planar cross-stratified sands and gravels, rippled sands and massive stratified gravels, interpreted as delta topsets. LFA3 caps the section and was probably deposited by migratory channels on the delta surface (Nemec et al., 1999). Sands in the delta top-sets (LFA3) were sampled for OSL, specifically from: (i) medium to coarse sand (Sr) from a channel fill (T3ALDO01: Fig 8D); and (ii) a thin (<0.1 m) unit of horizontally stratified coarse sand (Sh) (T3ALDO02) bound by units of coarser outwash sand and gravel (Fig. 8C). These two OSL samples yielded ages of 20.2 ± 3.5 ka (Fig. 2f; T3ALDO01) and 27.9 ± 4.7 ka (Fig. 2G; T3ALDO02). There was therefore a discrepancy between the OSL ages even though the samples were taken from the upper part of the same section. This potentially reflects the different depositional settings of the two samples, whereby T3ALDO01 (Fig. 2f; Fig. 8D) was deposited under lower-energy conditions than T3ALDO02 (Fig. 2g; Fig. 8C), which facilitated a greater opportunity for sunlight exposure prior to burial; thus, the well bleached part of the partially-bleached D_e distribution was characterised using fewer grains.

Offshore stratigraphy: The seabed north of the Isle of Man was surveyed and shallow geophysical and geotechnical data were collected during Cruise JC106 of the RRS James Cook (Fig. 10B). Line A (Fig. 10A) was located 40 km east of the Isle of Man extending across the glaciotectonic axis of the Bride Moraine, and showed a thick sequence of acoustically dense, stratified glaciomarine muds (AFA1-4). The acoustic stratigraphy showed a basal opaque and probably dense unit with its uppermost structures upright and with lower angle dipping units similar in character to the diapric folds and thrusts of the glaciotectonised diamicton (AFA1a), which was often interbedded with outwash deposits (AFA1b) (Thomas, 1984). The top of AFA1a-b appears to be truncated by coastal or shoreface processes (Fig. 10A), as it is cross-cut by AFA5 for which vibrocore data show is Holocene marine sands. AFA 4 (Fig. 10A), and to a lesser extent, deeper units of AFA 3, show extensive folding and deformation of muds attributable to glacier submarginal stresses acting against the bedrock slope of the Isle of Man. The kinotectonic zone of the Bride Moraine formed at an ice margin associated with Zones 4 and 5, when the ice margin was either at or north and east of the moraine. The undeformed, less dense stratified muds of AFA3 were then deposited under glaciomarine conditions and not overridden by ice during subsequent ice-marginal retreat. Acoustically less dense, stratified Holocene muds (AFA5) then capped the sedimentary sequence.

Survey lines further north in the Solway Firth (Line B: Fig. 10B) reveal a deeper chaotic and dense deposit (AFA1a-c: Fig. 10C) that overlies an acoustically opaque bedrock surface. Vibrocore JC106-084VC confirms that these deposits represent an over-consolidated Irish Sea-type (Thomas et al., 2004) diamicton (AFA1a: Fig. 11A) probably interspersed with outwash deposits (AFA1b). This is then capped by an overconsolidated laminated glaciomarine mud with numerous drop-stones (AFA1c: Fig. 11B) that reflects deglaciation at a calving ice margin. This in turn is overlain by normally-consolidated glaciomarine muds that vibrocore samples show were devoid of dropstones (Fig. 11C). The restricted multibeam data suggest that AFA4 has been sculpted by subglacial processes into drumlinoid forms. Both AFA1c and AFA3 contain sparse foraminifera indicative of glaciomarine conditions. Relatively thin shelly sands of Holocene age cap the sequence (AFA5). The combined sequence of AFA1a/AFA1c/AFA3 records the deposition of a subglacial diamicton, followed by ice margin retreat via calving into a marine basin before a readvance deformed and streamlined the glaciomarine muds into subglacial bedforms. Retrieved foraminifera were insufficient in number for ^{14}C dating. Acoustic line C (Fig. 10B and D) extends northwards from the eastern Irish Sea mud-belt into the Solway Firth and confirms the broad distribution of lithofacies. Dense laminated glaciomarine muds (AFA3-4) filled and capped an undulating topography, but reaches greater thicknesses in the south. Descending into the Solway Firth, the laminated muds became restricted to smaller basins between a series of ridges. The ridges appear as dense acoustic units similar to AFA 1a-c (Line B: Fig. 10C, Fig. 11A), and probably represent a series of ice-marginal moraine ridges to the north of the Isle of Man. These ridges appear to record ice-marginal oscillations in the Solway Firth during the ice retreat to BL6 (Fig. 1).

3.7 The Galloway Hills, SW Scotland (Zone 7)

During the LGM, the Galloway Hills in SW Scotland formed the major centre of ice dispersal in southern Scotland (Charlesworth, 1927; Geikie, 1894). Ice flowed radially out to the northeast, to the east across northern England, to the northwest and west to Firth of Clyde, and to the south into the Solway Firth, feeding the ISIS (Finlayson, 2013). Eight CN ages have been obtained from granite boulder at two sites near the former ice divide: four from Glen Trool (McCarroll et al., 2010) and four from Gadlach Brae (Ballantyne et al., 2013). These ages have been recalibrated here using a locally-derived 10Be production rate (LLPR; Table 5). Two ages (GT-03 and GB-02) represent statistically-distinct outliers, attributed by Ballantyne et al. (2013) to former sediment cover over the sampled boulders. The remaining three samples for Glen Trool (GT-01, GT-2.1 and GT-2.2) produced an uncertainty-weighted mean age of 15.4 ± 0.7 ka, and those for Gadlach Brae yielded an uncertainly-weighted mean age of 15.2 ± 0.8 ka. As these sampled boulders were obtained near the former ice divide, they indicate the timing of deglaciation shortly before the final disappearance of ice from this centre of ice dispersion. These CN ages therefore constrain the

ultimate retreat of the ice margin (BL7: Fig. 1) in SW Scotland after deglaciation of the NISB (Zone 6).

3.8 Bayesian Age Modelling the deglaciation of the Northern Irish Sea Basin

Bayesian analysis produced a conformable age model for the ice-marginal retreat sequence (Fig. 12A) with an overall agreement index of 84 % exceeding the >60 % threshold advocated by (Bronk Ramsey, 2009a). Five measurements were handled in the modelling as outliers: the OSL ages T4ABER01, T4BALH02 and T3JURB02, and the recalibrated TCN ages GB-02 and GT-03 previously regarded as affected by shielding (Ballantyne et al., 2013; McCarroll et al., 2010). The modelled ages (Table 6) suggest that ice in the NISB retreated 150 – 200 km from the coast of North Wales (BL1: 21.3 ± 1.0 k) to the Galloway Hills (BL6: 15.8 ± 0.8 ka) in ~4 ka. The OSL ages from Aber Ogwen provide the lower constraint on the NISB morpho-stratigraphic model (Zone 1). Low altitude sites on the Isle of Man (Cregneash and Turkeyland) constrain the deglaciation of the south of the island (Zone 2), and form the basis for the modelled boundary limit 2 (BL2) of 20.6 ± 0.6 ka. In the central valley of the Isle of Man, T3BALH02 was rejected as an outlier; thus, T3BALH01 provided the chronological control for the establishment of an ice-dammed lake (Zone 3) constraining BL3 (20.2 ± 0.7 ka). The OSL ages for the Orrisdale outwash sandur (T3ORIS01) and Dog Mills proglacial basin (T3DOGM01) constrain the timing of ice margins at the Bride moraine (Zone 4) to 19.6 ± 0.8 ka (BL4). Zones 5 and 6 contain more complicated parts of the prior model used in the Bayesian analysis (Fig. 12A), because the precise association and relative order of geochronology from Jurby, Gutterby and Aldoth is uncertain. Several versions of the modelling were undertaken varying the order and grouping of the age information from those three locations (Table 6). A Bayesian model (not shown) using the chronological data from the three sites as a single Phase (excluding T3GUTT01), essentially an unordered group of ages, produced conformable model (69%) a single boundary age of 18.9 ± 1.0 ka for Zone 5/6 (Table 6), the Scottish Readvance (Livingstone et al., 2010c). The higher agreement index (84%: Fig. 12A and Table 6) was achieved by grouping Jurby and Gutterby (Zone 5) as a Phase that predated the dating information from Aldoth (Zone 6) (Fig. 12). This model experiment suggests that Zone 5 constrained by OSL dating at Gutterby (excluding T3GUTT01) and Jurby represents the ice margin (BL5) at 19.2 ± 0.8 ka, and was associated with readvances of 2 – 3 km on the Isle of Man. In addition, Zone 6 is constrained by OSL dating at Aldoth and represents an ice margin (BL6) at 18.2 ± 1.1 ka, which is an age estimate for the Scottish Readvance (Livingstone et al., 2010c). There is very little difference between these two model scenarios: one linking the three locations around a boundary age of 18.9±1.0 ka and the other identifying two boundaries ages that overlap within uncertainties at 19.2 ± 0.8 and 18.2 ± 1.1 ka. The offshore sector positioned to the north of the Isle of Man in the Solway Firth (Zone 6) shows evidence of probable moraines and former ice margins. However, it failed to yield any dateable materials and so CN ages from the Southern Uplands (Scotland) constrain the ultimate deglaciation of the NISB to before 15.5 ± 0.7 ka (BL7).

4. DISCUSSION

Here we constrain the chronology for ice retreat in the central and eastern sector of the NISB. The new chronology provides timings for a series of readvances of the ice margin, including for sites evidencing the Scottish Readvance limit and reveals the pace of ice margin retreat in the NISB stepping on to land and into SW Scotland. Bayesian modelling of the geochronology indicates that ice margins retreated in the ISB an axial distance of 190 km at an average net rate of 54 m a^{-1} between 21.4 ± 1.0 ka and 15.5 ± 0.6 ka. The distances advanced by the ice margin can in part be assessed, but the precise distances covered during preceding retreat phases is impossible to gauge, thus the distances discussed are net rates. Net ice retreat was faster from the Llŷn Peninsula to the central Isle of Man at rates of 80 – 180 m a^{-1}, and then slowed to 20 m a^{-1} across the northern Isle of Man (BL3 – 4) before stabilizing at net retreat rates around 15 - 20 m a^{-1} in the terrestrial hinterlands of southern Scotland. The faster net retreat rates (80 – 180 m a^{-1}) were similar to the faster rates on the northern Llŷn Peninsula where the ice front was less constrained by trough geometry (84 – 139 m a^{-1}) (Smedley et al., 2017a). The slower net retreat rates (13 – 20 m a^{-1}) experienced in the NISB were similar to those reconstructed for the southern Llŷn Peninsula (8 – 41 m a^{-1}) (Smedley et al., 2017a) and southern Irish coast (26 m a^{-1}; Small et al. in review). Ice retreat rates across the NISB suggest that stabilisation occurred where the ice was pinned against the bedrock obstruction of the Isle of Man, and led to a series of ice-marginal oscillations at 19.8 – 18.2 ka, which left stratigraphical evidence for a series of standstill events and short distance (<1km) readvances of the ice margin (Thomas et al., 2004).

The CN ages obtained for upland settings on the Isle of Man and Cumbria do not directly constrain ice-marginal positions, but constrain potentially the thinning of ice in the ISB during retreat. The boulder age (T3BARR01) of 25.0 ± 1.4 ka from the summit (475 m) of South Barrule (Isle of Man) is of a similar age to the timing obtained for maximum extent of the ISIS at the Celtic Sea 25.1 – 24.5 ka cal. BP (Praeg et al., 2015) and 26 – 25 ka on the Isles of Scilly (Smedley et al., 2017b). The Celtic Sea advance of the ISIS has been suggested to have been a rapid and short-lived event (Chiverrell et al., 2013) that was followed by retreat to the south coast of Ireland by 26.3 – 23.9 ka (Small et al., under review) and the Llŷn Peninsula by 23.9 – 20.3 ka (Smedley et al., 2017a). Rapid retreat of this nature is likely to have been accompanied by significant drawdown of the ice stream surface. Taken at face value, the boulder CN age from the Isle of Man suggest ice thinning on the Isle of Man between ~25 and 19 ka to an elevation of 385 m, though caution is required in attaching significant to a single CN age. Assuming that the oldest of the Black Combe boulders was probably affected by nuclide inheritance, the calculating the average of the remaining pair of boulder ages at 260 m (20.7 ± 1.1 ka) supports ice thinning at this time. The ages for ice thinning in the mountains of the Isle of Man and Cumbria are older than previously published ages ~17.4 ka for ice free conditions in the Cumbrian Mountains (Ballantyne, 2010; Ballantyne et al., 2009; Wilson

and Lord, 2014; Wilson et al., 2013), but similar to equivalent data from Wales and Ireland where the summits had emerged by 20 - 19 ka in Snowdonia (Hughes et al., 2016) and by 24 – 21 ka in southeast Ireland (Ballantyne and Stone, 2015).

The late stage readvances in the Solway Lowlands, Isle of Man and the coastal lowlands of Cumbria were accompanied realignment of ice flow directions (Livingstone et al., 2010d). Geomorphological and stratigraphical investigations (Livingstone et al., 2010d; Merritt and Auton, 2000) suggested an ice limit that linked the evidence at Jurby, Annaside - Gutterby and Holme St Cuthbert, but was unconstrained by chronological control. The new OSL and CN ages provided here addresses this in part by confirming the relationship between ice-marginal positions at these three sites. Notwithstanding some overlap in the uncertainties for the ages at these three sites, there is synchrony between the Jurby, Gutterby and Aldoth positions with boundary limit modelled ages of 19.2 ± 0.8 ka (BL5) and 18.2 ±1.1 ka (BL6) (Fig. 12A). The parsimonious solution to the dating evidence from Jurby, Gutterby and Aldoth is that they represent a single event dated to 18.9 ± 1.0 ka thus constraining for the first time the age of the Scottish Readvance. It is equally possible that Aldoth and BL6 postdate the Jurby – Gutterby cluster with a Boundary Limit age of 18.2 ± 1.0 ka (BL6). There is stratigraphical evidence for repeated still-stands and oscillations of the ice margin that range in scale from a few 10s of metres to more substantial (2 – 3 km) readvances during decline of the ISIS (Thomas et al., 2004). Linking of ice marginal positions between Cumbria and the Isle of Man must remain tentative, but given that the ages presented here overlap in uncertainties it is equally possible that either Jurby, Gutterby and Aldoth formed a single synchronous ice margin at 18.9 ± 1.0 ka or that Jurby, Gutterby and Aldoth represent individual and potential separate readvances of the ice margin in the period 19.2 ± 0.8 to 18.2 ± 1.1 ka. The stratigraphy at each site shows they were each substantial (>1 km) advances of the ice margin within a relatively short period of time (1 - 2 ka). Regardless, this timing is interesting with respect to the chronology for ice margin retreat in adjacent regions. South of the Lake District, retreat of ice margins into north Lancashire has been constrained to 18.4 ± 0.8 ka (Chiverrell et al., 2016; Telfer et al., 2009; Wilson et al., 2013). East of the Carlisle Lowlands, the Tyne Gap Ice Stream draining east to the North Sea has a deglacial chronology for the Tyne headwaters that suggests progressive retreat from 18.7 to 17.1 ka . On the Lune and Eden watershed, CN ages from the Shap granite erratic train suggest deglaciation of the Vale of Eden by ~17.3 ka (Wilson et al., 2013). Thus, the Scottish readvance appears to have occurred either slightly before or early during the final deglaciation of much of Lake District and Tyne Gap ice.

The readvances and oscillations in the NE ISB have been compared previously with the series of ice margin advances recorded on the northeast coast of Ireland (McCabe, 2008). These were constrained by ^{14}C dating of marine microfauna (see Ballantyne and Cofaigh, 2017; McCabe, 2008 for detail) and comprise: (1) deglaciation of the NW ISB inferred from ice-free conditions at Kilkeel

Steps and Cooley Point (Fig.1); (2) the Clogher Head readvance constrained by readvance stratigraphical evidence and ages determined for Port, and subsequent retreat ages at Cranfield Point, Linns and Rathcor (Fig. 1); and (3) the Killard Point readvance is dated directly at Killard Point (Fig. 1) and bracketed by the ^{14}C dating at Linns and Rathcor and deglacial chronology from Rough Island (Fig. 1). This sequence of events forms a logical prior model for the Bayesian modelling of the retreat chronology in northeast Ireland (Fig. 12B). That model was conformable, contained no outlier ages and produced an overall agreement index of 106.1. The retreat sequence of the NW ISB (Fig. 12B) constrains deglaciation to shortly after 19.8 ±0.8 ka cal. BP, the Clogher Head Readvance to 18.7 ± 0.2 ka cal. BP and the Killard Point Readvance to 17.4 ± 0.3 ka cal. BP. Comparing the two Bayesian models (Fig. 12) suggests that BL5 at 19.2 ± 0.8 ka (BL5) broadly corresponds to the Clogher Head Readvance (McCabe, 2008). The Killard Point Readvance at 17.4 ± 0.3 ka cal. BP appears to lack an equivalent dated margin in the NE ISB, but does overlap with the Scottish Readvance (BL6) age range 18.2 ± 1.0 ka when Aldoth is treated as a separate Phase in the Bayesian modelling. The series of ridges present on the seafloor of the Solway Firth are also potentially equivalent to the Killard Point Readvance moraine, but currently lack dating control.

Following the short-lived advance of the ISIS into the Celtic Sea, the ice experienced overall ice-marginal retreat in the southern ISB that was punctuated by still-stands and oscillations, recorded from south to north along the coastlines of Ireland and Wales (Smedley et al., 2017a). During the ice retreat across the Llŷn Peninsula in the southern ISB, faster (e.g. 84 - 118 m a^{-1}) and shorter-lived phases of retreat (over centennial timeframes) occurred during periods of relatively stable climate These appear to have been driven by internal dynamics as the ISIS experienced a widening of the calving margin and a deepening of the trough (Smedley et al., 2017a). The new data presented here for ice retreat in the NISB north of the Llŷn Peninsula suggests that calving margin width continued to drive faster retreat rates (80 - 180 m a^{-1}) from North Wales (BL1: 21.2 ± 1.0 ka) to the Central Valley of the Isle of Man (BL2: 20.7 ± 0.7 ka), while external forcing (e.g. climate, RSL and SST) was unchanged (Fig. 13). The calving width then narrowed as the ISIS wrapped around the Isle of Man. This phase stabilised the ice front from ~20 to 19 ka (BL3 to BL5), with evidence for at least ten ice-marginal oscillations (Thomas et al., 2004) in relatively quick succession (ca. 1 ka) as the ISIS developed a terrestrially-terminating ice margin. These oscillations included the Orrisdale and Scottish advances and were similar in character to the centennial-scale oscillations recorded on the Llŷn Peninsula (Smedley et al., 2017a). This period of ice stability coincided with both stable climatic and oceanic conditions (Fig. 13 and the later stages of ice thinning in the mountains of the Isle of Man, Wales (Hughes et al., 2016), Lake District and southern Ireland (Ballantyne and Stone, 2015). The ice front then retreated from the NISB and into SW Scotland as air temperatures north of ~45 °N warmed in response to increased summer insolation (Fig. 13C), (Fig. 13). The responses of ice in this northeast sector of the ISB during H1

ca. 17.4 ka may be reflected in BL6 and also in the form of moraine ridges on the seafloor in the Solway Firth, but these landforms remain undated. Overall, the new chronology presented here suggests that ice-marginal retreat in the NISB was driven by a wider calving margin before the ice front became pinned by the Isle of Man and stabilised. The numerous and substantial ice-marginal oscillations experienced prior to this were probably driven by internal readjustments of the ice mass, which emphasises the importance of hypsometry on ice margin stability and oscillations. Once the air temperatures north of ~45 °N began to increase in response to summer insolation, it appears that a warming climate (Fig. 13C) (Bintanja et al., 2005) conditioned ice-marginal retreat out of the ISB and into SW Scotland.

5. CONCLUSIONS

Ice retreat in the northern ISB was more rapid (80 180 m a^{-1}) in southern sectors when ice margins retreated northwards from the Llŷn Peninsula to the Central Valley on the Isle of Man at ca. 20 ka. Average retreat rates then slowed to 13 – 20 m a^{-1} when the ice margin oscillated northwards across the northern Isle of Man and lowland Cumbria and experienced small- and large-scale retreat-readvance cycles before retreating northwards into the Galloway Hills in SW Scotland. CN ages obtained for the summits of the Isle of Man and Cumbrian Mountains overlap with the rapid retreat of ice from maximum limits in the Celtic Sea (Praeg et al., 2015; Smedley et al., 2017a; Smedley et al., 2017b). Although limited confidence can be placed on single CN ages, the older CN ages from South Barrule (Isle of Man) and Black Combe (Cumbria) possibly reflect the fact that ice thinning here was commensurate with the rapid retreat that followed the short-lived advance of the ISIS to maximum limits. New ages from multiple positions along ice limits (Livingstone et al., 2010) attributed to the Scottish Readvance (Trotter et al., 1937) constrain it the period 19.2 ± 0.8 to 18.2 ± 1.1 ka. The evidence for readvance of the ice margin at Jurby, Gutterby and Aldoth is unequivocal, but was accompanied by numerous other smaller scale oscillations and standstills of the ice margin, for example those elsewhere on the Cumbrian coast (Trotter et al., 1937) and those within the Orrisdale complex on the Isle of Man (Thomas et al., 2004). The new chronology suggests that it is possible the Scottish Readvance was a regionally penecontemporaneous event in the Cumbrian lowlands and the northern Isle of Man, and predated advance limits (possibly linked with H1) in the north of Ireland. Evidence for ice-marginal readvances and/or oscillations around the time of H1 may be preserved on the seafloor of Solway Firth, north of the Scottish Readvance limit, but currently undated.

Variations in ice retreat rates in the NISB support suggestions that internal ice dynamics responding to a wider calving margin and deeper trough coincide with faster retreat rates. The feasibility of the timing and scale of marginal oscillations during deglaciation in response to internal and external forcing could be tested using ice sheet modelling experiments. The subsequent slowing of ice-marginal retreat across the northern Isle of Man coincided with a reduced calving

front, a normal bedslope and a pinning point, in addition to the development of a terrestrially-terminating ice margin. Ultimately, the rapid deglaciation of the NISB from the Solway Firth into the Galloway Hills coincided with climate warming, probably driven by increased summer insolation, which overrode the internal controls on retreat. Overall, this new retreat sequence highlights the importance of internal dynamics in controlling ice retreat rates in the Irish Sea, but also documents the final demise of the ice in the NISB which occurs at the same time as climate warming north of ~45 °N.

ACKNOWLEDGEMENTS

This paper was supported by a Natural Environment Research Council consortium grant (BRITICE-CHRONO NE/J008672/1). The cosmogenic analyses were supported by the NERC Cosmogenic Isotope Analysis Facility allocation 9155.1014. Thanks are due to the staff at the SUERC AMS Laboratory, East Kilbride for 10Be isotope measurements. H. Wynne is thanked for etching the quartz grains for OSL dating. The Master and crew of the RRS James Cook are thanks for their endeavours during Cruise JC106. Manx National Heritage is thanked for permission for access and sampling the erratic boulders on South Barrule. Landowners and the Operators at Turkeyland (C.Kniveton Ltd), Ballaharra (Corletts) and Aldoth (D A Harrison) Quarries are thanks for their support and for allowing access for sampling.

REFERENCES

Arnold, L.J., Roberts, R.G. (2009) Stochastic modelling of multi-grain equivalent dose (De) distributions: Implications for OSL dating of sediment mixtures. Quaternary Geochronology 4, 204-230.

Balco, G., Stone, J.O., Lifton, N.A., Dunai, T.J. (2008) A complete and easily accessible means of calculating surface exposure ages or erosion rates from 10Be and 26Al measurements. Quaternary Geochronology 3, 174-195.

Ballantyne, C.K. (2010) Extent and deglacial chronology of the last British-Irish Ice Sheet: Implications of exposure dating using cosmogenic isotopes. Journal of Quaternary Science 25, 515-534.

Ballantyne, C.K., Cofaigh, C.Ó., (2017) The last Irish Ice Sheet: extent and chronology, Advances in Irish Quaternary Studies. Springer, pp. 101-149.

Ballantyne, C.K., Rinterknecht, V., Gheorghiu, D.M. (2013) Deglaciation chronology of the Galloway Hills Ice Centre, southwest Scotland. Journal of Quaternary Science 28, 412-420.

Ballantyne, C.K., Stone, J.O. (2015) Trimlines, blockfields and the vertical extent of the last ice sheet in Southern Ireland. Boreas 44, 277-287.

Ballantyne, C.K., Stone, J.O., Fifield, L.K. (2009) Glaciation and deglaciation of the SW Lake District, England: implications of cosmogenic 36Cl exposure dating. Proceedings of the Geologists' Association 120, 139-144.

Bintanja, R., van de Wal, R.S.W., Oerlemans, J. (2005) Modelled atmospheric temperatures and global sea levels over the past million years. Nature 437, 125-128.

Bradley, S.L., Milne, G.A., Shennan, I., Edwards, R. (2011) An improved glacial isostatic adjustment model for the British Isles. Journal of Quaternary Science 26, 541-552.

Bronk Ramsey, C. (2009a) Bayesian analysis of radiocarbon dates. Radiocarbon 51, 337-360.

Bronk Ramsey, C. (2009b) Dealing with outliers and offsets in radiocarbon dating. Radiocarbon 51, 1023-1045.

Bronk Ramsey, C., Lee, S. (2013) Recent and Planned Developments of the Program Oxcal. Radiocarbon 55, 720-730.

Buck, C.E., Cavanagh, W.G., Litton, C.D. (1996) Bayesian Approach to Interpreting Archaeological Data.

Chadwick, R.A., Jackson, D.I., Barnes, R.P., Kimbell, G.S., Johnson, H., Chiverrell, R.C., Thomas, G.S.P., Jones, N.S., Riley, N.J., Pickett, E.A., Young, B., Holliday, D.W., Ball, D.F., Molyneux, S.G., Long, D., Power, G.M., Roberts, D.H. (2001) Geology of the Isle of Man and its offshore area. British Geological Survey Research Report.

Child, D., Elliott, G., Mifsud, C., Smith, A.M., Fink, D. (2000) Sample processing for earth science studies at ANTARES. Nuclear Instruments and Methods in Physics Research, Section B: Beam Interactions with Materials and Atoms 172, 856-860.

Chiverrell, R.C., Burke, M.J., Thomas, G.S.P. (2016) Morphological and sedimentary responses to ice mass interaction during the last deglaciation. Journal of Quaternary Science 31, 265-280.

Chiverrell, R.C., Thrasher, I.M., Thomas, G.S.P., Lang, A., Scourse, J.D., van Landeghem, K.J.J., McCarroll, D., Clark, C.D., Ó'Cofaigh, C., Evans, D.J.A., Ballantyne, C.K. (2013) Bayesian modelling the retreat of the Irish Sea Ice Stream. Journal of Quaternary Science 28, 200-209.

Clemmensen, L.B., Houmark-Nielsen, M. (1981) Sedimentary features of a Weichselian glaciolacustrine delta. Boreas 10, 229-245.

Cohen, J.M. (1979) Deltaic sedimentation in glacial lake Blessington, County Wicklow, Ireland. Proc. INQUA symposium on genesis and lithology of Quaternary deposits, Zurich, 10-20 September 1978. Moraines and varves: origin, genesis, classification, 357-368.

Darwin, C. (1848) On the transportal of erratic boulders from a lower to a higher level. Quarterly Journal of the Geological Society of London 4, 315-323.

Edge, M.J., Hart, J., Pointon, K., (1990) The sequences at Aber Ogwen and Glan-y-mor-isaf, in: Addison, K., Edge, M.J., Watkins, R. (Eds.), The Quaternary of North Wales: Field Guide. Quaternary Research Association, Coventry, pp. 119-130.

Evans, D.J.A., Benn, D.I. (2004) A Practical Guide to the Study of Glacial Sediments. A Practical Guide to the Study of Glacial Sediments.

Fabel, D., Ballantyne, C.K., Xu, S. (2012) Trimlines, blockfields, mountain-top erratics and the vertical dimensions of the last British-Irish Ice Sheet in NW Scotland. Quaternary Science Reviews 55, 91-102.

Gustavson, T.C., Ashley, G.M., Boothroyd, J.C. (1975) Depositional sequences in glaciolacustrine deltas. Glaciofluvial and Glaciolacustrine Sedimentation 23, 264-280.

Haapaniemi, A.I., Scourse, J.D., Peck, V.L., Kennedy, H., Kennedy, P., Hemming, S.R., Furze, M.F.A., Pienkowski, A.J., Austin, W.E.N., Walden, J., Wadsworth, E., Hall, I.R. (2010) Source, timing, frequency and flux of ice-rafted detritus to the Northeast Atlantic margin, 30-12 ka: Testing the Heinrich precursor hypothesis. Boreas 39, 576-591.

Huddart, D. (1970) Aspects of Glacial Sedimentation in the Cumberland Lowland. Aspects of Glacial Sedimentation in the Cumberland Lowland.

Huddart, D. (1971) A relative glacial chronology from the tills of the Cumberland lowland. Proceedings of the Cumberland Geological Society 3, 21-32.

Huddart, D. (1977) Gutterby Spa - Annaside Banks Moraine and St. Bees Moraine. The Isle of Man, Lancashire Coast and Lake District.

Huddart, D., (1991) The glacial history and glacial deposits of the north and west Cumbrian lowlands, in: Ehlers, J., Gibbard, P.L., Rose, J. (Eds.), Glacial deposits of Great Britain and Ireland. Balkema, Rotterdam. Balkema, Rotterdam, pp. 151-167.

Huddart, D., Glasser, N.F. (2002) Quaternary of Northern England. GCR Series 25, 745.

Hughes, P.D., Glasser, N.F., Fink, D. (2016) Rapid thinning of the Welsh Ice Cap at 20-19 ka based on 10Be ages. Quaternary Research (United States) 85, 107-117.

Jackson, D.I., Jackson, A.A., Evans, D., Wingfield, R.T.R., Barnes, R.P., Arthur, M.J. (1995) United Kingdom Offshore Regional Report: The Geology of the Irish Sea.

Jopling, A.V., Walker, R.G. (1968) Morphology and origin of ripple-drift cross-lamination, with examples from the Pleistocene of Massachusetts. Journal of Sedimentary Petrology 38, 971-984.

Kohl, C.P., Nishiizumi, K. (1992) Chemical isolation of quartz for measurement of in-situ -produced cosmogenic nuclides. Geochimica et Cosmochimica Acta 56, 3583-3587.

Lal, D. (1991) Cosmic ray labeling of erosion surfaces: in situ nuclide production rates and erosion models. Earth and Planetary Science Letters 104, 424-439.

Lamplugh, G.W., (1898) Geological Survey of England and Wales. Isle of Man. Geologically surveyed by G.W. Lamplugh 1892-97 ... Scale of one inch to a statute mile. Ordnance Survey Office, Southampton.

Lamplugh, G.W. (1903) The geology of the Isle of Man. Memoir of the Geological Survey of the United Kingdom.

Livingstone, S.J., Cofaigh, C.Ó., Evans, D.J.A. (2008) Glacial geomorphology of the central sector of the last British-Irish Ice sheet. Journal of Maps 4, 358-377.

Livingstone, S.J., Cofaigh, C.Ó., Evans, D.J.A. (2010a) A major ice drainage pathway of the last British-Irish ice sheet: The Tyne Gap, Northern England. Journal of Quaternary Science 25, 354-370.

Livingstone, S.J., Evans, D.J.A., Cofaigh, C.Ó., Hopkins, J. (2010b) The Brampton kame belt and Pennine escarpment meltwater channel system (Cumbria, UK): Morphology, sedimentology and formation. Proceedings of the Geologists' Association 121, 423-443.

Livingstone, S.J., Evans, D.J.A., Ó'Cofaigh, C. (2010c) Re-advance of Scottish ice into the Solway Lowlands (Cumbria, UK) during the Main Late Devensian deglaciation. Quaternary Science Reviews 29, 2544-2570.

Livingstone, S.J., Evans, D.J.A., Ó'Cofaigh, C., Davies, B.J., Merritt, J.W., Huddart, D., Mitchell, W.A., Roberts, D.H., Yorke, L. (2012) Glaciodynamics of the central sector of the last British-Irish Ice Sheet in Northern England. Earth-Science Reviews 111, 25-55.

Livingstone, S.J., Ó'Cofaigh, C., Evans, D.J., Palmer, A. (2010d) Sedimentary evidence for a major glacial oscillation and proglacial lake formation in the Solway Lowlands (Cumbria, UK) during Late Devensian deglaciation. Boreas 39, 505-527.

McCabe, A.M. (2008) Glacial geology and geomorphology: the landscapes of Ireland. Dunedin Academic Press, Edinburgh.

McCabe, A.M., Clark, P.U., Clark, J., Dunlop, P. (2007) Radiocarbon constraints on readvances of the British–Irish Ice Sheet in the northern Irish Sea Basin during the last deglaciation. Quaternary Science Reviews 26, 1204-1211.

McCabe, A.M., Knight, J., McCarron, S. (1998) Evidence for Heinrich event 1 in the British Isles. Journal of Quaternary Science 13, 549-568.

McCarroll, D., Stone, J.O., Ballantyne, C.K., Scourse, J.D., Fifield, L.K., Evans, D.J.A., Hiemstra, J.F. (2010) Exposure-age constraints on the extent, timing and rate of retreat of the last Irish Sea ice stream. Quaternary Science Reviews 29, 1844-1852.

Merritt, J.W., Auton, C.A., (2000) An outline of the lithostratigraphy and depositional history of Quaternary deposits in the Sellafield district, west Cumbria, Proceedings of the Yorkshire Geological and Polytechnic Society. Geological Society of London, pp. 129-154.

Nemec, W., (2009) Aspects of Sediment Movement on Steep Delta Slopes, Coarse-Grained Deltas, pp. 29-73.

Nemec, W., Lønne, I., Blikra, L.H. (1999) The Kregnes moraine in Gauldalen, west-central Norway: Anatomy of a Younger Dryas proglacial delta in a palaeofjord basin. Boreas 28, 454-476.

Pantin, H.M., Hughes, M.J., Wilson, J.B. (1978) Quaternary sediments from the north-east Irish Sea: Isle of Man to Cumbria. Bulletin of the Geological Survey of Great Britain 64, 1-43.

Praeg, D., McCarron, S., Dove, D., Cofaigh, C.O., Scott, G., Monteys, X., Facchin, L., Romeo, R., Coxon, P. (2015) Ice sheet extension to the Celtic Sea shelf edge at the Last Glacial Maximum. Quaternary Science Reviews 111, 107-112.

Roberts, D.H., Dackombe, R.V., Thomas, G.S.P. (2007) Palaeo-ice streaming in the central sector of the British-Irish Ice Sheet during the Last Glacial Maximum: evidence from the northern Irish Sea Basin. Boreas 36, 115-129.

Rodnight, H., Duller, G.A.T., Wintle, A.G., Tooth, S. (2006) Assessing the reproducibility and accuracy of optical dating of fluvial deposits. Quaternary Geochronology 1, 109-120.

Smedley, R.K., Chiverrell, R.C., Ballantyne, C.K., Burke, M.J., Clark, C.D., Duller, G.A.T., Fabel, D., McCarroll, D., Scourse, J.D., Small, D., Thomas, G.S.P. (2017a) Internal dynamics condition centennial-scale oscillations in marine-based ice-stream retreat. Geology 45, 787-790.

Smedley, R.K., Scourse, J.D., Small, D., Hiemstra, J.F., Duller, G.A.T., Bateman, M.D., Burke, M.J., Chiverrell, R.C., Clark, C.D., Davies, S.M., Fabel, D., Gheorghiu, D.M., McCarroll, D., Medialdea, A., Xu, S. (2017b) New age constraints for the limit of the British-Irish Ice Sheet on the Isles of Scilly. Journal of Quaternary Science 32, 48-62.

Smith, N.D., Ashley, G.M. (1985) Proglacial lacustrine environment. Glacial sedimentary environments, 135-216.

Stone, J.O. (2000) Air pressure and cosmogenic isotope production. Journal of Geophysical Research: Solid Earth 105, 23753-23759.

Telfer, M.W., Wilson, P., Lord, T.C., Vincent, P.J. (2009) New constraints on the age of the last ice sheet glaciation in NW England using optically stimulated luminescence dating. Journal of Quaternary Science 24, 906-915.

Thomas, G.S.P., (1977) The quaternary of the Isle of Man, in: Tooley, M.J. (Ed.), The Quaternary history of the Irish Sea. Steel House Press, Liverpool. Geological Journal Special Issue, pp. 155-178.

Thomas, G.S.P. (1984) The origin of the glacio-dynamic structure of the Bride Moraine, Isle of Man. Boreas 13, 355-364.

Thomas, G.S.P., Chiverrell, R., Huddart, D. (2004) Ice-marginal depositional responses to readvance episodes in the Late Devensian deglaciation of the Isle of Man. Quaternary Science Reviews 23, 85-106.

Thomas, G.S.P., Chiverrell, R.C., Huddart, D., Long, D., Roberts, D.H., (2006) The Ice Age, in: Chiverrell, R.C., Thomas, G.S.P. (Eds.), A New History of the Isle of Man: Volume 1 Evolution of the natural landscape. Liverpool University Press, Liverpool, pp. 126-219.

Thomas, G.S.P., Connaughton, M., Dackombe, R.V. (1985) Facies Variation in a Late Pleistocene Supraglacial Outwash Sandur from the Isle-of-Man. Geological Journal 20, 193-213.

Trotter, F.M., Hollingworth, S.E. (1932) The Glacial Sequence in the North of England. Geological Magazine 69, 374-380.

Trotter, F.M., Hollingworth, S.E., Eastwood, T., Rose, W.C.C. (1937) Gosforth District. Geological Survey Memoir, England and Wales, Sheet 37.

Van Landeghem, K.J.J., Wheeler, A.J., Mitchell, N.C. (2009) Seafloor evidence for palaeo-ice streaming and calving of the grounded Irish Sea Ice Stream: Implications for the interpretation of its final deglaciation phase. Boreas 38, 111-131.

Williams, G.D., Brabham, P.J., Eaton, G.P., Harris, C. (2001) Late Devensian glaciotectonic deformation at St Bees, Cumbria: a critical wedge model. Journal of the Geological Society 158, 125-135.

Wilson, P., Lord, T. (2014) Towards a robust deglacial chronology for the northwest England sector of the last British-Irish Ice Sheet. North West Geography 14.

Wilson, P., Lord, T., Rodés, Á. (2013) Deglaciation of the eastern Cumbria glaciokarst, northwest England, as determined by cosmogenic nuclide (10Be) surface exposure dating, and the pattern and significance of subsequent environmental changes. Cave and Karst Science 40, 22-27.

Xu, S., Dougans, A.B., Freeman, S.P.H.T., Schnabel, C., Wilcken, K.M. (2010) Improved 10Be and 26Al-AMS with a 5 MV spectrometer. Nuclear Instruments and Methods in Physics Research, Section B: Beam Interactions with Materials and Atoms 268, 736-738.

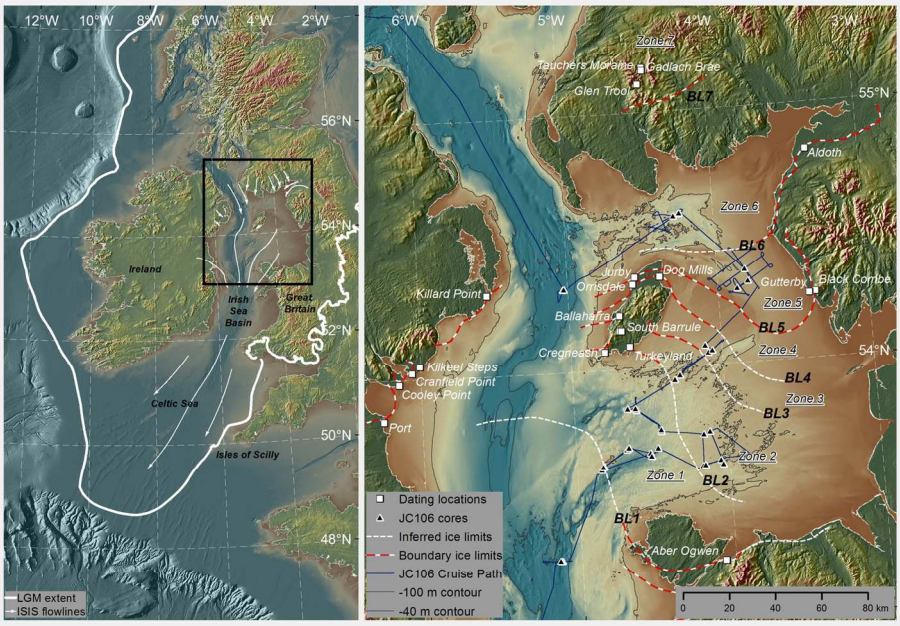

Fig. 1. Location and context of the northern Irish Sea Basin plotted on Nextmap™ and EMODnet topographical data (http://www.emodnet-hydrography.eu/). This shows inferred ice margins (red and white) including the possible extent of the calving margins. Triangles denote cores and geophysical survey lines (black dashed lines) taken on the cruise JC106 and the locations of dating sites. The zones (1-7) and boundaries (BL1 to 7) used the chronological model are identified.

147x106mm (300 x 300 DPI)

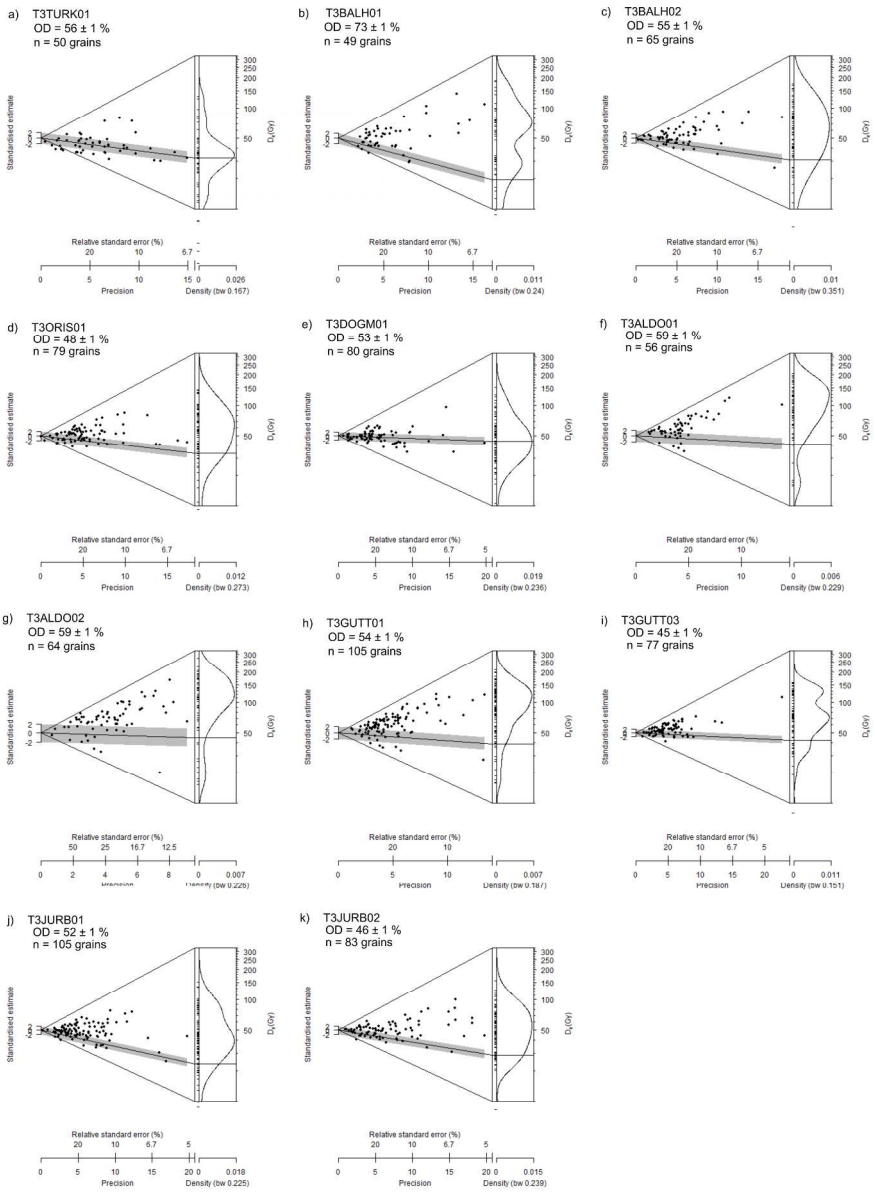

Fig. 2. Abanico plots of the De values determined for OSL dating, where the grey shading shows the CAM or MAM De for each distribution. Note that sample T3DOGM01 was analysed using microhole analysis rather than single grains (i.e. up to four grains in each hole due to a grain size of 150 – 180 μm) and so the CAM provides a maximum OSL age for this sample.

256x340mm (300 x 300 DPI)

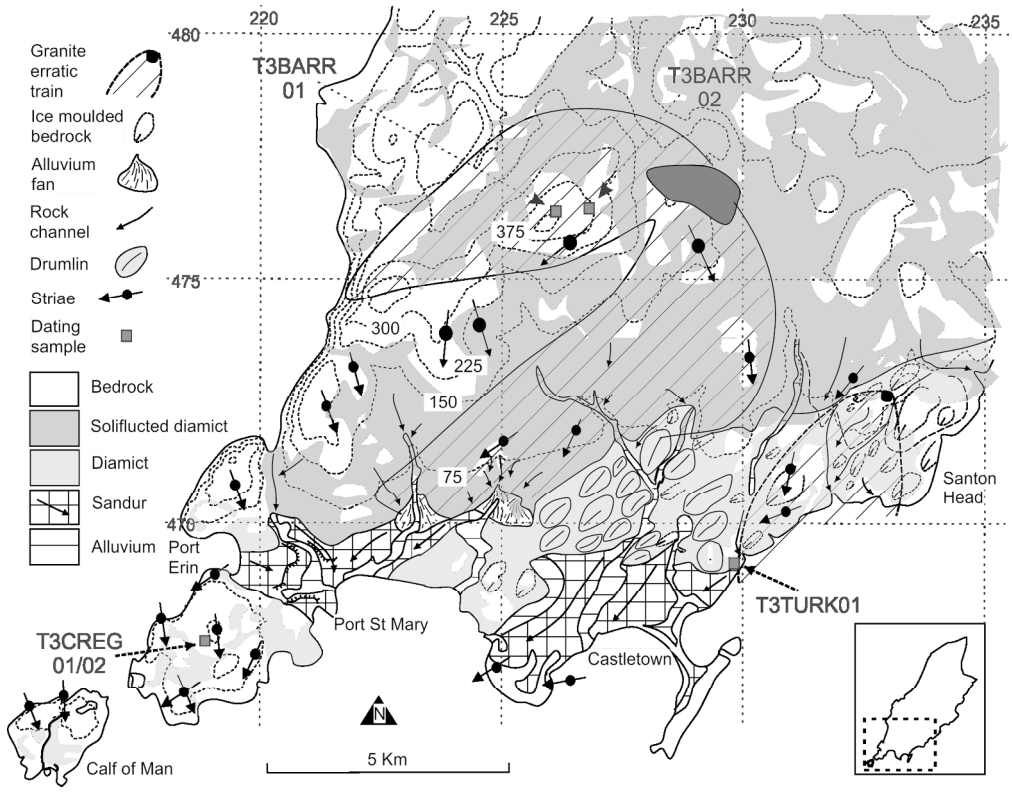

Fig. 3. Glacial geomorphology of the south of the Isle of Man and a 5 km Ordnance Survey grid (after Thomas et al., 2006; Roberts et al., 2006) showing the locations of samples T3CREG01 and T3CREG02, T3TURK01 and T3BARR01 and T3BARR02.

166x129mm (300 x 300 DPI)

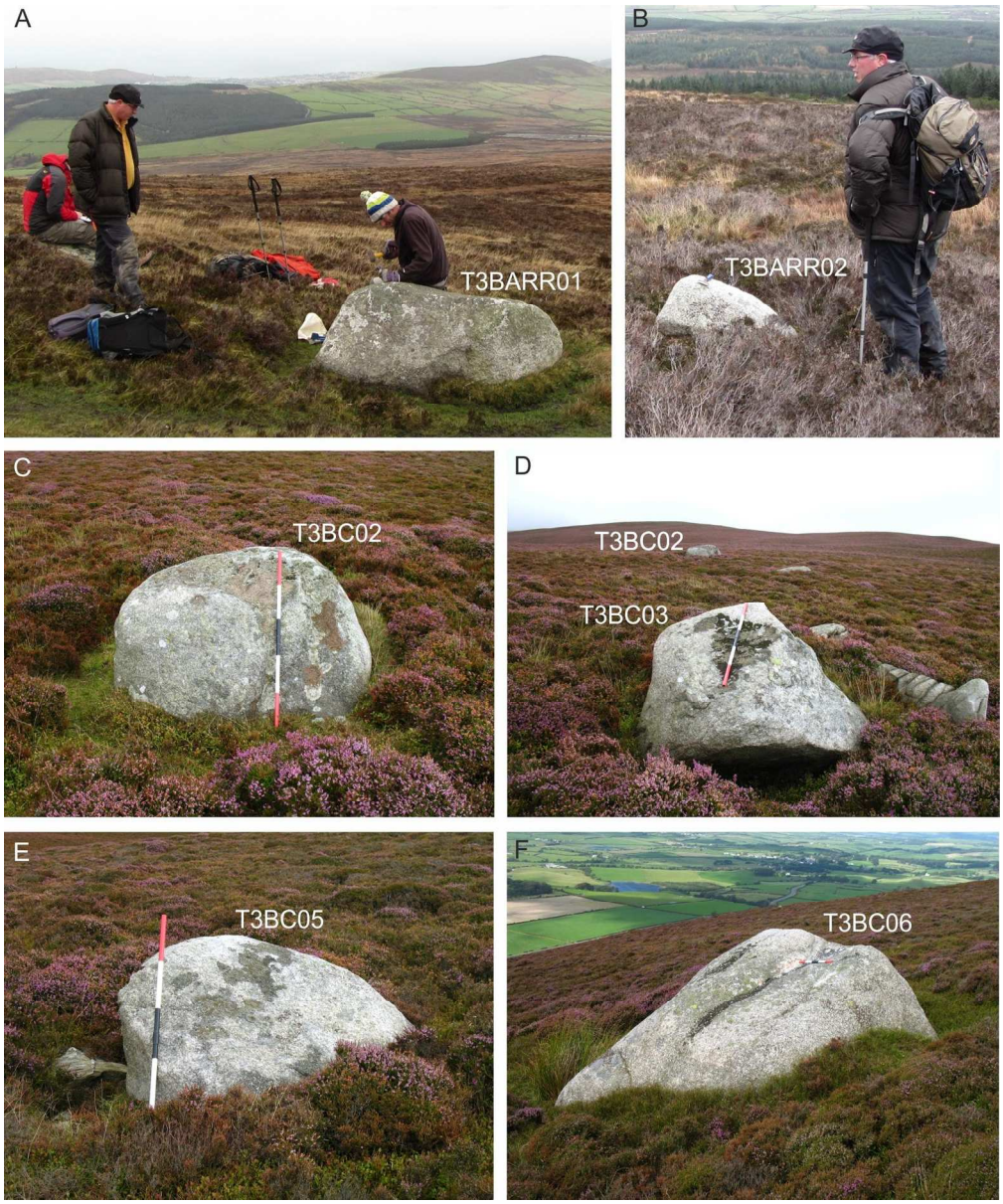

Fig. 4. Cosmogenic nuclide samples: A. T3BARR01 from the summit of South Barrule, B. T3BARR02 from the flanks of South Barrule on the Isle of Man. C-F. Samples from Black Combe in coastal Cumbria, NW England.

453x544mm (96 x 96 DPI)

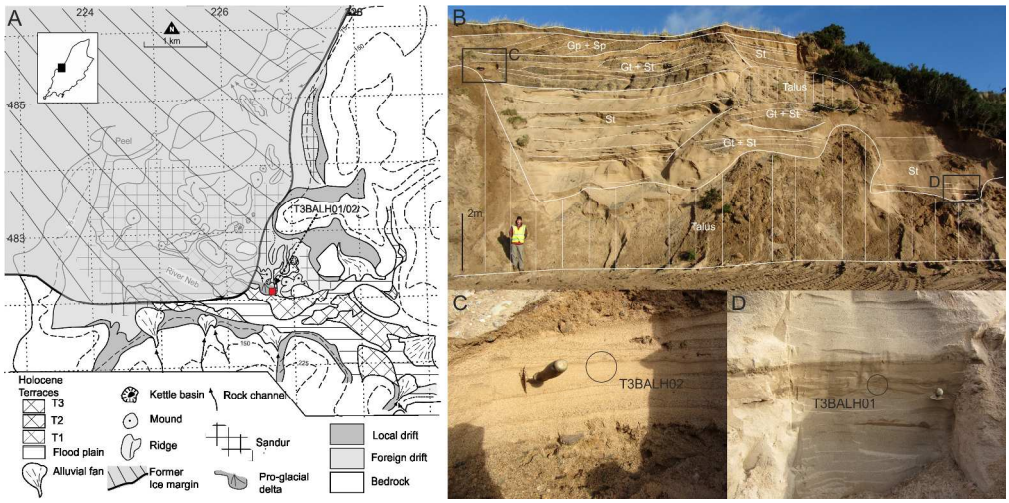

Fig. 5. Glacial geomorphology of the Peel Embayment, central Isle of Man (after Thomas et al., 2006) and a 1 km Ordnance Survey grid, showing the locations of samples T3BALH01 and T3BALH02 (a). Quarry section photographs, summary stratigraphy and lithofacies at Ballaharra quarry on 7/11/2013 (b) and samples T3BALH01 (c) and T3BALH02 (d).

269x133mm (300 x 300 DPI)

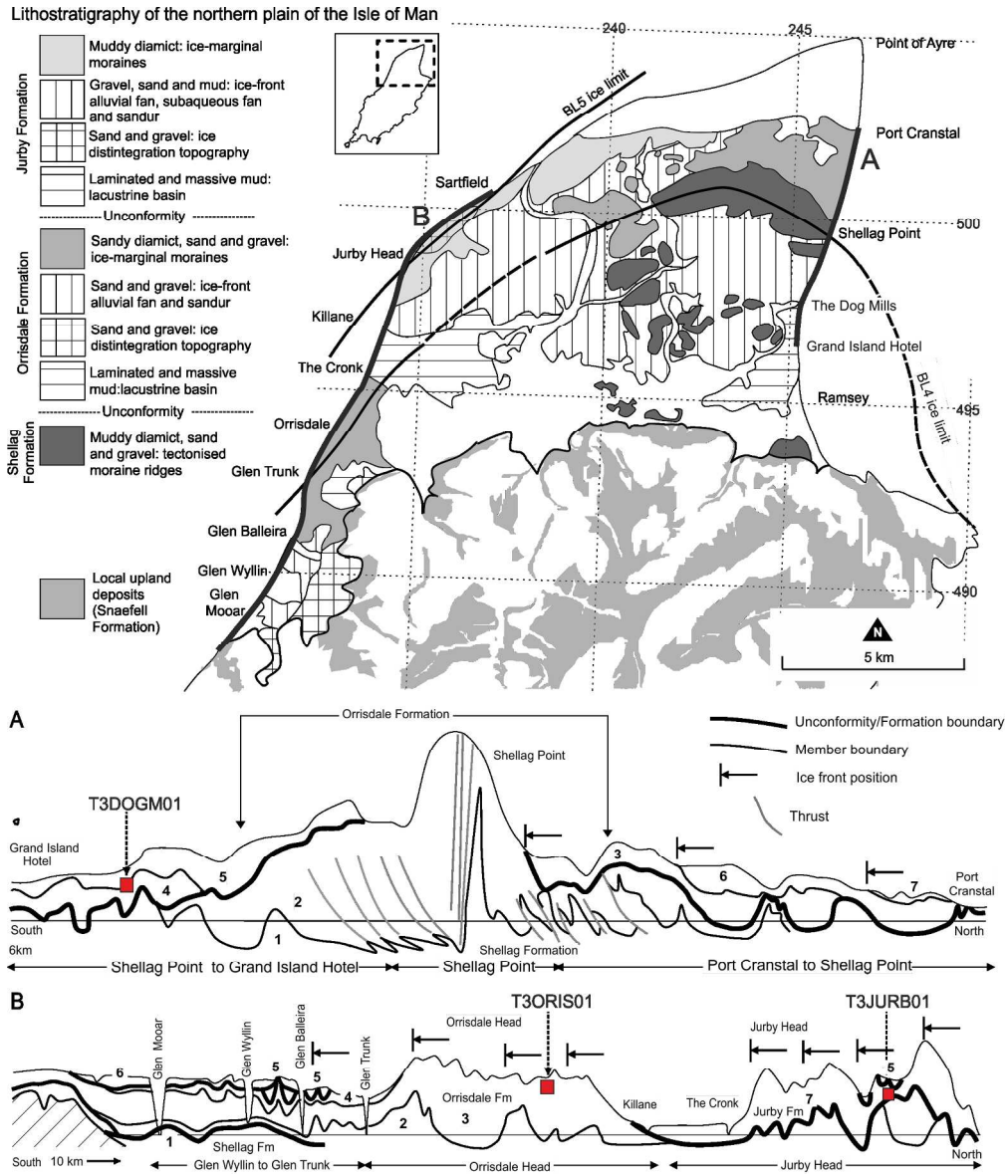

Fig. 6. Lithostratigraphy of the Northern Plain of the Isle of Man with a 5 km Ordnance Survey grid. Summary stratigraphy and lithofacies assemblages on the east and west coasts of the Northern Plain of the Isle of Man, identifying the OSL samples from Orrisdale (T3ORIS01), Dog Mills (T3DOGM01) and Jurby (T3JURB01, T3JURB02).

203x237mm (300 x 300 DPI)

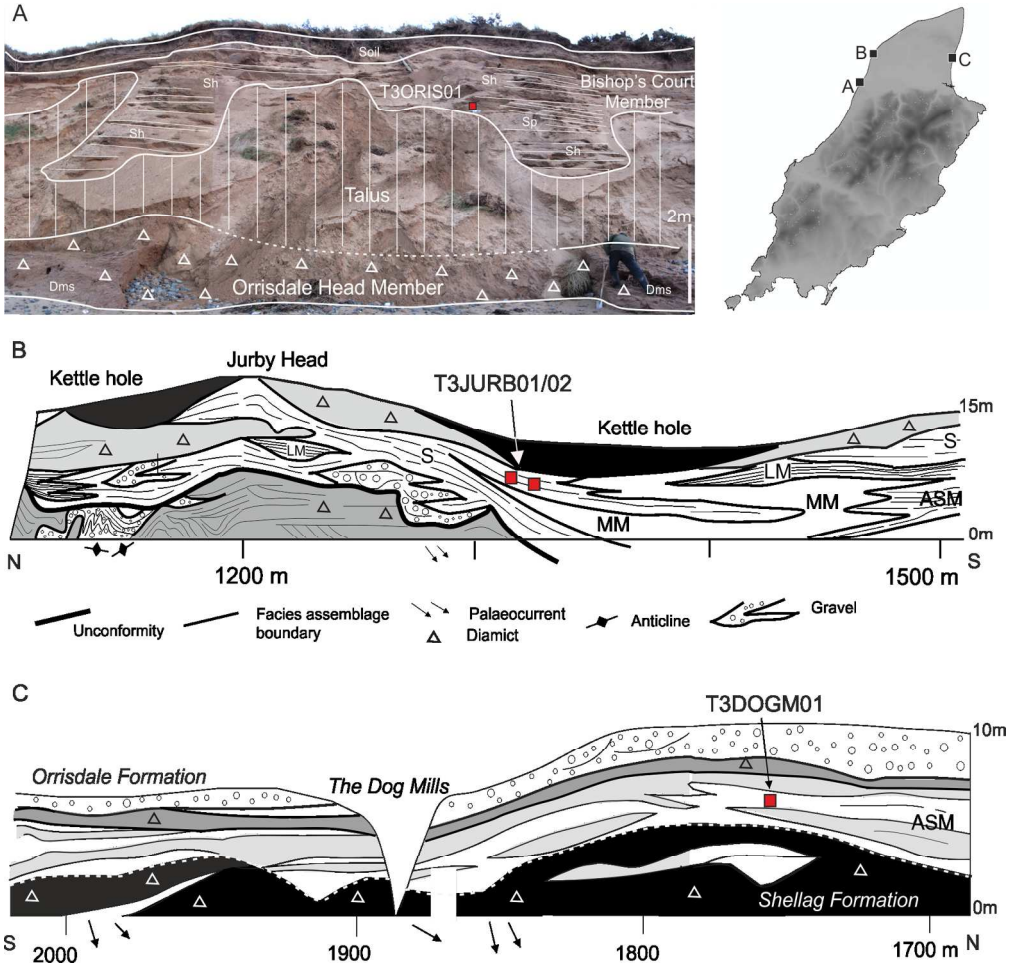

Fig 7. Detailed stratigraphy and lithofacies assemblages identifying the OSL samples from Orrisdale photographed 7/11/2013 (T3ORIS01), Dog Mills (T3DOGM01) and Jurby (T3JURB01, T3JURB02) (after Thomas et al., 2006). Lithofacies codes: S - sand, ASM - alternating sand and mud, LM - laminated mud, MM - massive mud.

161x154mm (300 x 300 DPI)

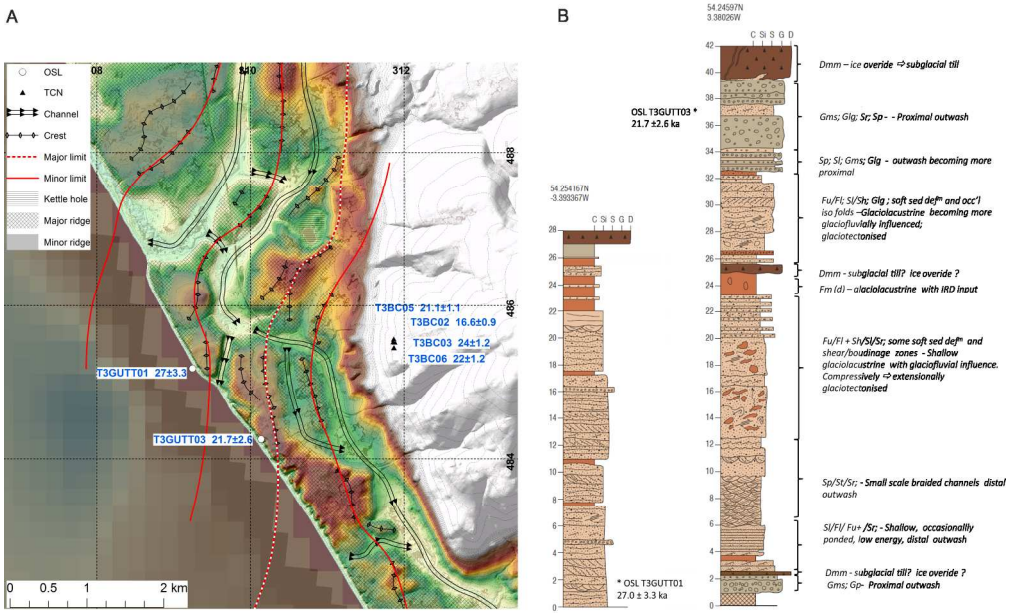

Fig. 8. A) Geomorphology and sampling around Gutterby-Annaside Banks and Black Combe. B) Stratigraphical logs from the Gutterby sections T3GUTT01 and T3GUTT03.

224x143mm (300 x 300 DPI)

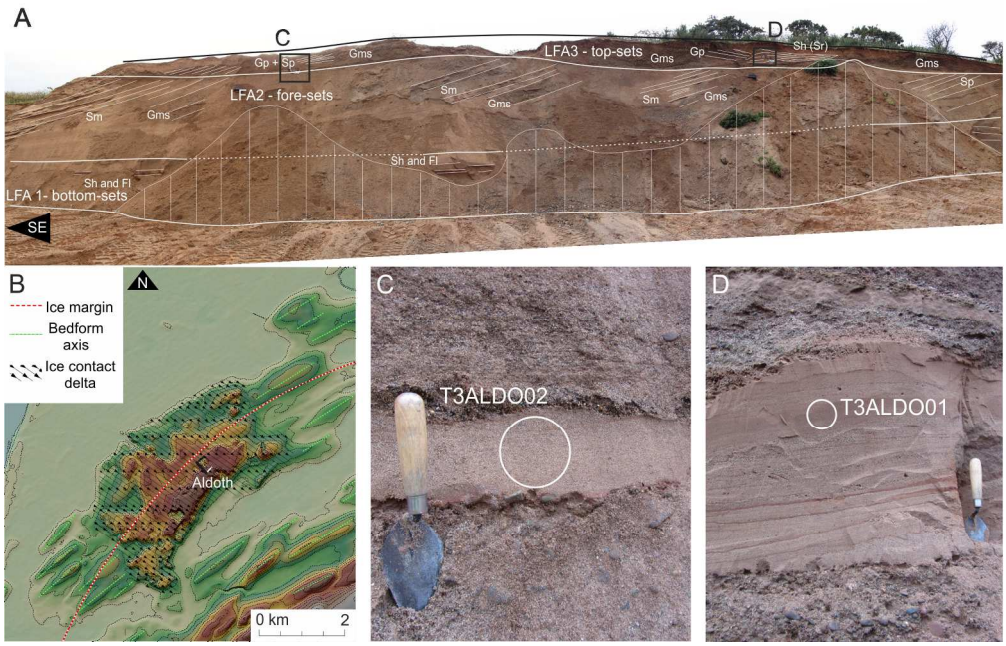

Fig. 9. The Holme St Cuthbert ice contact delta on the Scottish Readvance limit. A. NW-SE Quarry face at Aldoth Quarry in December 2013. B. Aldoth Quarry in the Holme St Cuthbert ice contact delta complex. C and D OSL samples T3ALDO02 and T3ALDO01 respectively.

195x125mm (300 x 300 DPI)

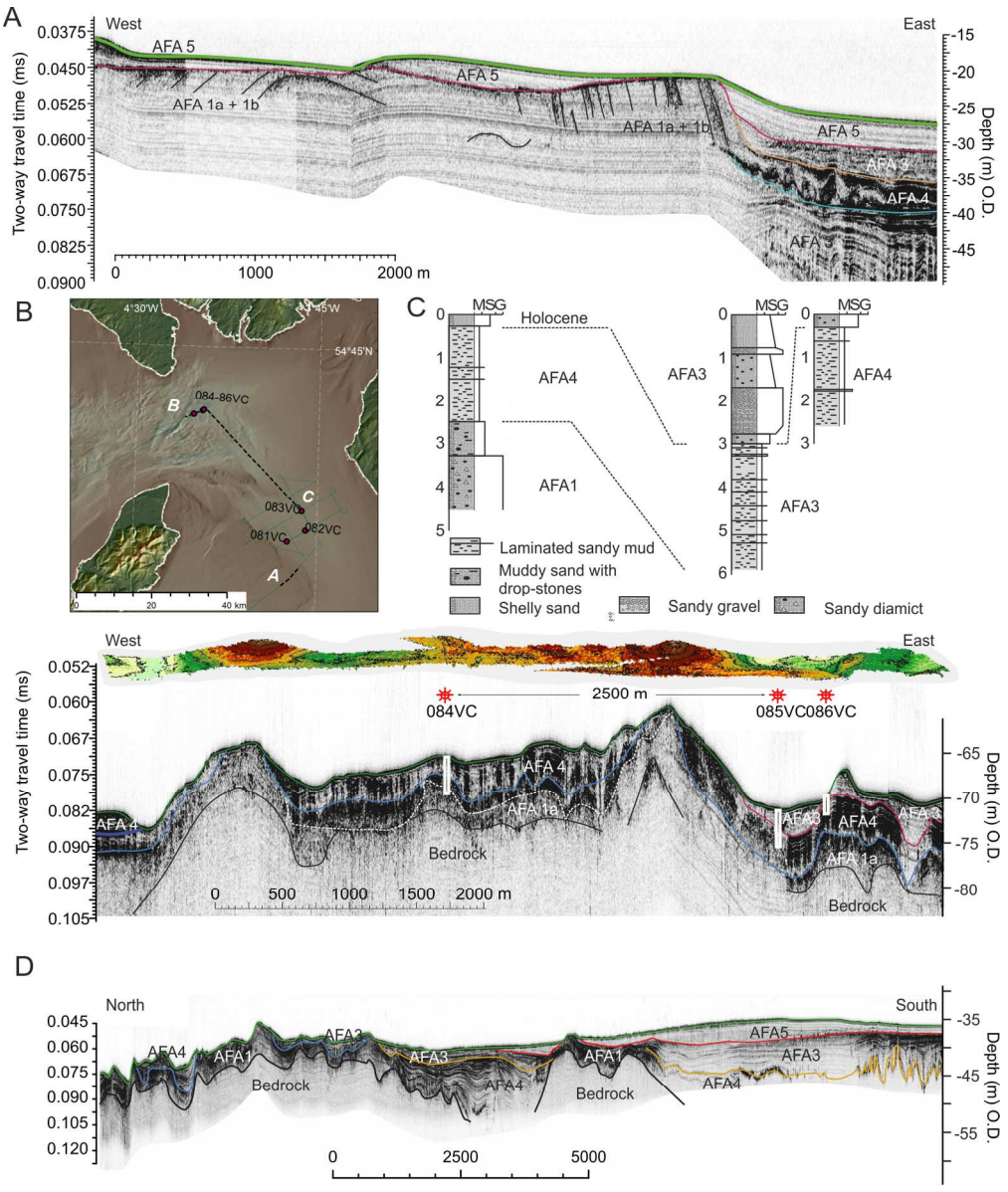

Fig. 10. Sub-bottom profiler data and acoustic facies associations (AFA). A. East of the Isle of Man (Line A). B. The location of the JC106 cruise (green), the cores and transects shown for lines A-C. C. The Solway Firth (Line B) including the vibrocore logs. D. A south-to-north transect from the eastern Irish Sea mud basin and Solway Firth (Line C).

156x184mm (300 x 300 DPI)

Fig. 11. Lithofacies examples from key acoustic facies sampled from vibrocore JC106-084VC from the Solway Firth.

97x126mm (300 x 300 DPI)

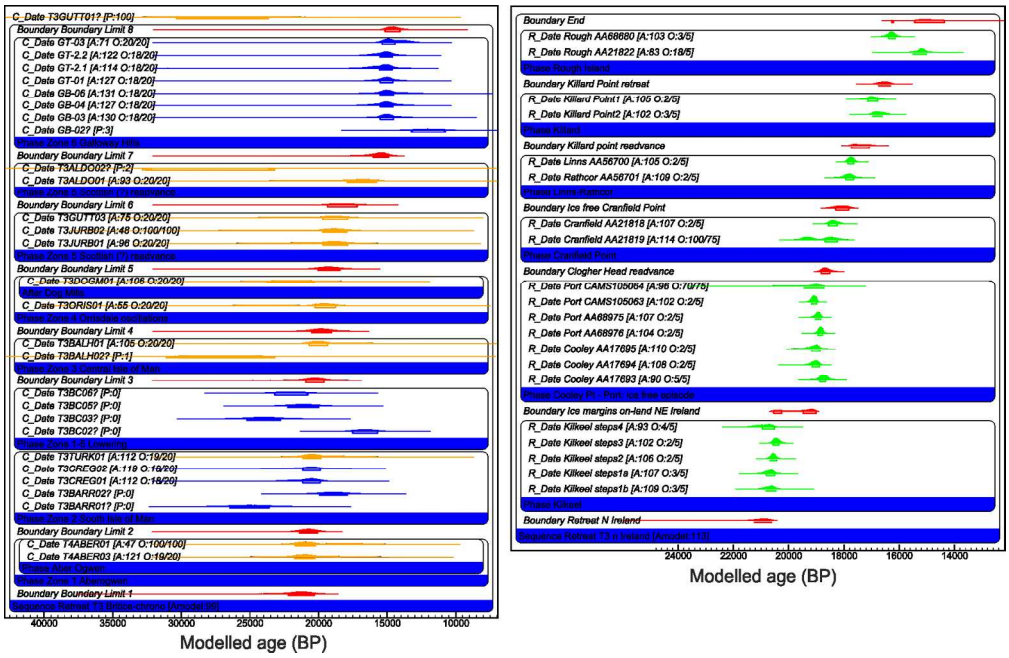

Fig. 12. Bayesian models for the dating of ice retreat across A) the northeast Irish Sea Basin and B) northeast Ireland, and the model structure using OxCal keywords that defines the relative order of events (Ramsey, 2009a). Each distribution (hollow) represents the relative probability of each age estimate with posterior density estimate (solid) generated by the modelling. Shown are 14C ages (green), OSL ages (orange), CN ages (blue) and modelled boundary ages (Red). Absolute outliers are denoted by '?', also listing the agreement index for individual ages.

159x103mm (300 x 300 DPI)

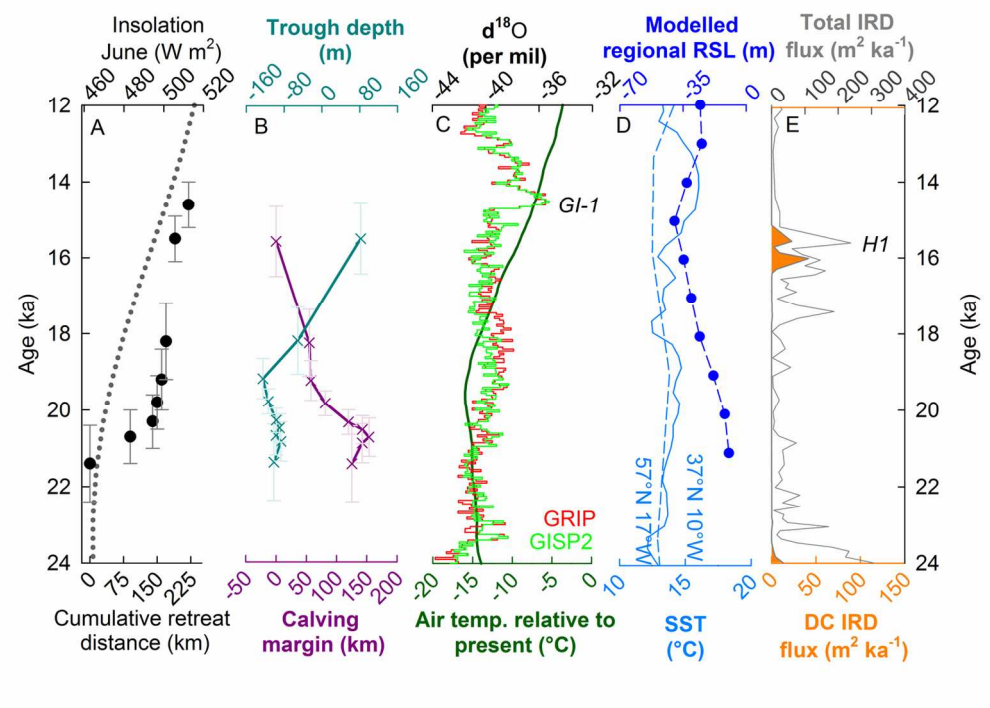

Fig. 13. A: The boundary ages from the Bayesian model against axial retreat distance plotted with summer insolation for 60°N (Berger and Loutre, 1991). B: Likely calving margin widths and trough depths estimated as mean of 10 % deepest depths from the EMODnet bathymetry (http://www.emodnet-hydrography.eu/) plotted against the boundary ages. C: d18O concentrations and Greenland Interstadials (GI) from the Greenland ice cores (Rasmussen et al. (2014) and modelled surface air temperatures relative to the present for land masses north of ~45°N (Bintanja et al., 2005). D: SST records determined for the North Atlantic using alkenones at 37°N 10°W (Bard, 2002) plotted using the updated age model of Bard et al. (2004) and from Ocean Drilling Project (ODP) site 982 at 57°N 17°W (Lawrence et al., 2009). E: Observed global eustatic sea level (ESL ± 1 σ) (Lambeck et al. (2014) and modelled RSL for Anglesey derived from the glacial isostatic adjustment (GIA) model of Bradley et al. (2011). F: The dolomitic carbon (DC) and total ice rafted debris (IRD) flux records from the OMEX2K marine core (Haapaniemi et al., 2010). Heinrich Event H1 is highlighted (after Bond et al., 1993).

139x99mm (300 x 300 DPI)

Table 1. Acoustic facies associations (AFA) and the supporting lithostratigraphy from vibrocores for seismic lines in the northern ISB (Fig. 1). These AFAs are used as annotation on seismic lines 1 – 3 on Fig. 8.

Acoustic Facies	Lithostratigraphy	Environment and processes
AFA 1a	Overconsolidated sandy matrix supported pebbly diamicton (Dmm)	Irish Sea Till, subglacial diamict
AFA 1b	Overconsolidated sands (Sh) and gravels (Gm, Gms), including planar and trough cross-stratified units (Gp, Sp, Gt, St)	Glaciofluvial outwash, occasionally tectonised and overconsolidated
AFA 1c	Overconsolidated occasionally laminated muds with dropstones (Dml)	Ice proximal outwash, affected by iceberg calving, overridden by ice
AFA 2	Sands and silts (Sh and Fl), normally-consolidated, often bedded (1-10mm) occasionally massive (Sm)	Ice proximal outwash, either subaerial or efflux jet discharge from the ice margin
AFA 3	Normally-consolidated, laminated muds, silts and clays (Fl)	Ice distal suspension rain-out in a subaqueous basin
AFA 4	Glacitectonised (AFA 3), laminated muds, silts and clays (Fl)	Ice distal suspension deformed and glacitectonised by advancing ice
AFA 5	Unconsolidated shelly sands and gravels	Holocene shell-hash, sands and gravels worked by marine currents

Table 2. Environmental dose-rates were determined using ICP-MS and ICP-AES analysis and in situ gamma spectrometry. The chemical concentrations are presented in the decimal points relevant for the detection limit. The grainsize for all samples was 212 – 250 μm, except for sample T3DOGM01 which was 150 – 180 μm. The dose-rates were calculated using the conversion factors of Guerin et al. (2011) and beta dose-rate attenuation factors of Guerin et al. (2012). Water contents were estimated considering the field and saturated water contents, and the environmental history for each sample; these values are expressed as a percentage of the mass of dry sediment. Cosmic dose-rates were determined after Prescott and Hutton (1994). Dose-rates were calculated using the Dose Rate and Age Calculator (DRAC; Durcan et al. 2015).

Sample	Depth (m)	Water content (%)	K (%)	Rb (ppm)	U (ppm)	Th (ppm)	Beta dose-rate (Gy/ka)	Gamma dose-rate (Gy/ka)	Cosmic dose-rate (Gy/ka)	Total dose-rate (Gy/ka)
T3TURK01	1.0	20 ± 5	1.1 ± 0.1	59.2 ± 5.9	1.44 ± 0.14	6.0 ± 0.6	0.87 ± 0.08	0.59 ± 0.04	0.18 ± 0.02	1.67 ± 0.09
T3BALH01	13.0	23 ± 5	0.9 ± 0.1	31.9 ± 3.2	0.76 ± 0.08	2.5 ± 0.3	0.62 ± 0.07	0.38 ± 0.02	0.05 ± 0.01	1.06 ± 0.07
T3BALH02	3.0	17 ± 5	0.8 ± 0.1	28.0 ± 2.8	0.59 ± 0.06	2.1 ± 0.2	0.57 ± 0.06	0.40 ± 0.03	0.14 ± 0.01	1.12 ± 0.07
T3ORIS01	5.0	17 ± 5	1.2 ± 0.1	30.1 ± 3.0	0.81 ± 0.08	2.5 ± 0.3	0.84 ± 0.09	0.44 ± 0.03	0.11 ± 0.01	1.40 ± 0.09
T3DOGM01	5.0	23 ± 5	1.5 ± 0.2	49.7 ± 5.0	1.53 ± 0.15	4.7 ± 0.5	1.10 ± 0.13	0.73 ± 0.05	0.11 ± 0.01	1.97 ± 0.14
T3JURB01	9.5	23 ± 5	1.0 ± 0.1	36.7 ± 3.7	0.85 ± 0.09	3.2 ± 0.3	0.69 ± 0.07	0.35 ± 0.02	0.07 ± 0.01	1.13 ± 0.07
T3JURB02	6.5	23 ± 5	1.1 ± 0.1	36.8 ± 3.7	0.72 ± 0.07	2.4 ± 0.2	0.73 ± 0.07	0.39 ± 0.03	0.09 ± 0.01	1.22 ± 0.08
T3GUTT01	20.0	30 ± 5	1.5 ± 0.2	61.5 ± 6.2	0.89 ± 0.09	3.0 ± 0.3	0.92 ± 0.09	0.49 ± 0.03	0.03 ± 0.00	1.44 ± 0.10
T3GUTT03	3.5	23 ± 5	1.5 ± 0.2	66.1 ± 6.6	0.96 ± 0.10	3.3 ± 0.3	0.99 ± 0.10	0.83 ± 0.05	0.13 ± 0.01	1.97 ± 0.11
T3ALDO01	1.0	20 ± 5	1.7 ± 0.2	53.5 ± 5.4	0.94 ± 0.09	3.5 ± 0.4	1.14 ± 0.13	0.71 ± 0.05	0.18 ± 0.02	2.04 ± 0.14
T3ALDO02	1.5	20 ± 5	1.1 ± 0.1	39.5 ± 4.0	0.88 ± 0.09	3.6 ± 0.4	0.78 ± 0.07	0.65 ± 0.04	0.17 ± 0.02	1.61 ± 0.09

Table 3. OSL analysis results, including the dose-recovery (DR) and overdispersion (OD).

Sample	Grain size (μm)	DR OD (%)	Total analysed	n	OD (%)	Age model	σ_b	D_e (Gy)	Age (ka)
T3TURK01	212 – 250	17	1,600	50	56 ± 1	CAM	-	32.0 ± 2.8	19.2 ± 2.0
T3BALH01	212 – 250	14	1,900	49	72 ± 1	MAM	0.25	19.6 ± 3.2	17.6 ± 3.1
T3BALH02	212 – 250	-	2,000	65	55 ± 1	MAM	0.25	30.5 ± 3.9	27.1 ± 3.8
T3ORIS01	212 – 250	10	3,800	94	48 ± 1	MAM	0.20	33.3 ± 3.7	23.8 ± 3.1
T3DOGM01	150 – 180	0	1,800	80	53 ± 1	CAM	-	44.2 ± 2.9	21.9 ± 1.9
T3JURB01	212 – 250	8	4,000	105	52 ± 1	MAM	0.20	23.5 ± 2.3	20.8 ± 2.4
T3JURB02	212 – 250	-	2,800	83	46 ± 1	MAM	0.20	28.6 ± 2.9	23.4 ± 2.8
T3GUTT01	212 – 250	0	7,300	105	54 ± 1	MAM	0.20	38.9 ± 4.0	27.0 ± 3.3
T3GUTT03	212 – 250	-	5,600	77	45 ± 1	MAM	0.20	42.6 ± 4.3	21.7 ± 2.6
T3ALDO01	212 – 250	15	2,400	56	59 ± 1	MAM	0.25	41.2 ± 6.6	20.2 ± 3.5
T3ALDO02	212 – 250	-	2,800	64	59 ± 1	MAM	0.25	45.0 ± 7.1	27.9 ± 4.7

Table 4. Sample information and exposure ages for the new TCN samples. Calculations were performed using the CRONUS-Earth online calculator developmental version; wrapper script 2.2, Main calculator 2.1, constants 2.2.1, muons 1.1.

Sample	Lat.	Long.	Alt. (m)	Thickness (cm)	Shielding[a]	^{10}Be conc. (at g^{-1})[b]	^{10}Be conc. ±	Exposure Age (ka)[c]
T3CREG01	54.07156	-4.77349	155	2.5	0.998	97548	2995	21.2 ± 1.2
T3CREG02	54.07156	-4.77349	155	3.8	1.000	95553	2580	20.9 ± 1.1
T3BARR01	54.1509	-4.6677	475	0.9	0.989	156340	4633	25.0 ± 1.4
T3BARR02	54.1507	-4.6548	385	2.4	0.995	108922	3169	18.9 ± 1.0
T3BC02	54.25763	-3.35291	260	2.4	1	88567	2614	16.6 ± 0.9
T3BC03	54.25768	-3.35315	255	3	1	124435	3049	24.0 ± 1.2
T3BC05	54.25798	-3.35308	255	4.2	1	108664	2811	21.1 ± 1.1
T3BC06	54.25698	-3.35303	255	3.4	1	114599	3324	22.0 ± 1.2

[a] Calculated using CRONUS calculator (Balco et al. 2008), available at: (http://hess.ess.washington.edu/math/general/skyline_input.php).
[b] Be analyses were standardised to NIST27900 with ^{10}Be/^{9}Be taken as 2.79 x 10^{-11}. A process blank correction of 5.89 ± 1.04 x 10^{-15} was applied to all samples. Concentrations rounded to nearest 100 atoms.
[c] Exposure ages calculated using CRONUS calculator developmental version; Wrapper script 2.2, Main calculator 2.1, Constants 2.2.1, Muons 1.1; http://hess.ess.washington.edu/math/al_be_v22/al_be_calibrate_v22.php; accessed 25/11/2015 (Balco et al. 2008), Lm scaling, assuming a density of 2.6 g cm^{-3}. Analytical uncertainties reported in parentheses.

Table 5. CN ages re-calculated using the LLPR. The calculations were performed using the CRONUS-Earth online calculator developmental version; wrapper script 2.3, Main calculator 2.1, constants 2.3, muons 1.1. The highlighted samples (*) were identified as outliers in the original studies. Note that in the original studies, Lm scaling factors were used by Ballantyne et al. (2013) while Du scaling factors were used by McCarroll et al. (2010).

Sample	Isotope	Published ages (ka)	Analytical uncert (ka)	Uncert. (ka)	LLPR ages (ka)	Uncert. (ka)	Original publication
GB-02	^{10}Be	12.0	1.1	1.2	12.0	1.2	Ballantyne et al. (2013)
GB-03	^{10}Be	14.7	1.0	1.2	14.8	1.2	Ballantyne et al. (2013)
GB-04	^{10}Be	15.0	0.6	0.9	15.1	0.9	Ballantyne et al. (2013)
GB-06	^{10}Be	14.7	1.2	1.4	14.7	1.4	Ballantyne et al. (2013)
GT-01	^{10}Be	14.1	0.6	1.8	15.1	0.9	McCarroll et al. (2010)
GT-2.1	^{10}Be	14.3	0.3	1.7	15.5	0.8	McCarroll et al. (2010)
GT-2.2	^{10}Be	14.3	0.5	1.8	15.3	0.8	McCarroll et al. (2010)
GT-03	^{10}Be	13.0	0.4	1.6	14.0	0.7	McCarroll et al. (2010)

Table 6. Modelled ages for each stage shown in bold and unmodelled OSL and CN ages (±1 σ). Ages marked "*" were identified as outliers and so did not influence the modelled outputs. On the left boundary ages with Zone 5/6 grouped as single Phase, and on the right boundary ages where Zone 5 and 6 were separate Phases.

Prior	Age (ka)	Prior	Age (ka)
Boundary Limit 1	21.4 ± 1.0	Boundary Limit 1	21.4 ± 1.0
Zone 1 North Wales		Zone 1 North Wales	
T4ABER01	18.1 ± 1.6	T4ABER01	18.1 ± 1.6
T4ABER03	20.2 ± 1.9	T4ABER03	20.2 ± 1.9
Boundary Limit 2	20.7 ± 0.7	Boundary Limit 2	20.7 ± 0.7
Zone 2 South Isle of Man		Zone 2 South Isle of Man	
T3BARR01*	25.0 ± 1.4	T3BARR01*	25.0 ± 1.4
T3BARR02*	18.9 ± 1.0	T3BARR02*	18.9 ± 1.0
T3CREG01	21.2 ± 1.2	T3CREG01	21.2 ± 1.2
T3CREG02	20.9 ± 1.1	T3CREG02	20.9 ± 1.1
T3TURK01	19.2 ± 2.0	T3TURK01	19.2 ± 2.0
T3BC02*	16.6 ± 0.9	T3BC02*	16.6 ± 0.9
T3BC03*	24.0 ± 1.2	T3BC03*	24.0 ± 1.2
T3BC05*	21.1 ± 1.1	T3BC05*	21.1 ± 1.1
T3BC06*	22.0 ± 1.2	T3BC06*	22.0 ± 1.2
Boundary Limit 3	20.3 ± 0.7	Boundary Limit 3	20.3 ± 0.7
Zone 3 Central Isle of Man		Zone 3 Central Isle of Man	
T3BALH01	18.5 ± 3.3	T3BALH01	18.5 ± 3.3
T3BALH02*	27.1 ± 3.8	T3BALH02*	27.1 ± 3.8
Boundary Limit 4	19.8 ± 0.7	Boundary Limit 4	19.8 ± 0.7
Zone 4 Orrisdale		Zone 4 Orrisdale	
T3ORIS01	23.8 ± 3.1	T3ORIS01	23.8 ± 3.1
T3DOGM01	<22.5 ± 2.2	T3DOGM01	<22.5 ± 2.2
Boundary Limit 5	18.9 ± 1.0	Boundary Limit 5	19.2 ± 0.8
Zone 5/6 Scottish Readvance		Zone 5 Jurby – Gutterby	
		T3JURB01	20.8 ± 2.4
T3JURB01	20.8 ± 2.4	T3JURB02	23.4 ± 2.8
T3JURB02	23.4 ± 2.8	T3GUTT03	21.7 ± 2.6
T3GUTT03	21.7 ± 2.6	Boundary Limit 6	18.2 ± 1.0
T3ALDO01	20.2 ± 3.5	Zone 6 Scottish Readvance	
T3ALDO02*	27.9 ± 4.7	T3ALDO01	20.2 ± 3.5
		T3ALDO02*	27.9 ± 4.7
Boundary Limit 7	15.5 ± 0.6	Boundary Limit 7	15.5 ± 0.6
Zone 7 Galloway Hills		Zone 7 Galloway Hills	
GB-02*	12.0 ± 1.2	GB-02*	12.0 ± 1.2
GB-03	14.8 ± 1.2	GB-03	14.8 ± 1.2
GB-04	15.1 ± 0.9	GB-04	15.1 ± 0.9
GB-06	14.7 ± 1.4	GB-06	14.7 ± 1.4
GT-01	15.1 ± 0.9	GT-01	15.1 ± 0.9
GT-2.1	15.5 ± 0.8	GT-2.1	15.5 ± 0.8
GT-2.2	15.3 ± 0.8	GT-2.2	15.3 ± 0.8
GT-03	14.0 ± 0.7	GT-03	14.0 ± 0.7
Boundary Limit 8 (End)	14.6 ± 0.6	Boundary Limit 8 (End)	14.6 ± 0.6

SUPPLEMENTARY MATERIAL

ICE MARGIN OSCILLATIONS DURING DEGLACIATION OF THE NORTHERN IRISH SEA BASIN

R.C. Chiverrell[1*], R.K. Smedley[1,2,3,], D. Small[4], C.K. Ballantyne[5], M.J. Burke[1], S.L. Callard[6], C.D. Clark[7], G.A.T. Duller[2], D.J.A. Evans[6], D. Fabel[8], K. van Landeghem[9], Stephen Livingstone[7], G.S.P. Thomas[1]. D.H. Roberts[6], M Saher[9], J.D. Scourse[10], P. Wilson[11]

[1]School of Environmental Sciences, University of Liverpool, Liverpool, UK
[2]Department of Geography and Earth Sciences, Aberystwyth University, Ceredigion, UK
[3]School of Geography, Geology and the Environment, Keele University, Keele, Staffordshire, UK
[4]School of Geographical and Earth Sciences, University of Glasgow, Glasgow, UK
[5]School of Geography and Sustainable Development, University of St Andrews, St Andrews, UK
[6]Department of Geography, Durham University, Durham, UK
[7]Department of Geography, University of Sheffield, Sheffield, UK
[8]Scottish Universities Environmental Research Centre, East Kilbride, UK
[9]School of Ocean Sciences, Bangor University, Menai Bridge, Anglesey, UK
10College of Life and Environmental Science, University of Exeter, Cornwall, UK
[11]School of Geography and Environmental Sciences, University of Ulster, Belfast, UK
(*E-mail: RCHIV@LIV.AC.UK)

BAYESIAN MODELLING CODE

```
Options()
 {
  BCAD=FALSE;

Delta_R("LocalMarine",0,0);

Curve("Marine13","Marine1
3.14c");
 };
 Plot()
 {
  Outlier_Model("T3-ISB
East", T(5), U(0,4), t);
  Sequence("Retreat T3
Britice-chrono")
  {
   Boundary("Boundary Limit
1")
   {
    color="Red";
   };
   Phase("Zone 1
Aberogwen")
   {
    Phase("Aber Ogwen")
    {
     C_Date("T4ABER03",
20200, 1900)
     {
      color="Orange";
      Outlier("Test", 0.2);
     };
     C_Date("T4ABER01",
18100, 1600)
     {
      color="Orange";
      Outlier("Test", 1);
     };
    };
   };
   Boundary("Boundary Limit
2")
   {
    color="Red";
   };
   Phase("Zone 2 South Isle
of Man")
   {
    C_Date("T3BARR01",
25000, 1400)
    {
     color="Blue";
     Outlier();
    };
    C_Date("T3BARR02",
18900, 1000)
    {
     Outlier();
     color="Blue";
    };
```

```
    C_Date("T3CREG01",
21200, 1200)
    {
     Outlier("Test", 0.2);
     color="Blue";
    };
    C_Date("T3CREG02",
20900, 1100)
    {
     Outlier("Test", 0.2);
     color="Blue";
    };
    C_Date("T3TURK01",
19200, 2000)
    {
     Outlier("Test", 0.2);
     color="Orange";
    };
   };
   Phase("Zone 1-5
Lowering")
   {
    C_Date("T3BC02",
16600, 900)
    {
     Outlier();
     color="Blue";
    };
    C_Date("T3BC03",
24000, 1200)
    {
     Outlier();
     color="Blue";
    };
    C_Date("T3BC05",
21100, 1100)
    {
     Outlier();
     color="Blue";
    };
    C_Date("T3BC06",
22000, 1200)
    {
     Outlier();
     color="Blue";
    };
   };
   Boundary("Boundary Limit
3")
   {
    color="Red";
   };
   Phase("Zone 3 Central
Isle of Man")
   {
    C_Date("T3BALH02",
27100, 3800)
    {
     color="Orange";
     Outlier();
    };
    C_Date("T3BALH01",
17600, 3100)
    {
     color="Orange";
     Outlier("Test", 0.2);
    };
   };
   Boundary("Boundary Limit
4")
   {
    color="Red";
   };
   Phase("Zone 4 Orrisdale
oscillations")
   {
    C_Date("T3ORIS01",
23800, 3100)
    {
     color="Orange";
     Outlier("Test", 0.2);
    };
    After("Dog Mills")
    {
     C_Date("T3DOGM01",
21900, 1900)
     {
      color="Orange";
      Outlier("Test", 0.2);
     };
    };
   };
   Boundary("Boundary Limit
5")
   {
    color="Red";
   };
   Phase("Zone 5 Scottish
(?) readvance")
   {
    C_Date("T3JURB01",
20800, 2400)
    {
     color="Orange";
     Outlier("Test", 0.2);
    };
    C_Date("T3JURB02",
23400, 2800)
    {
     color="Orange";
     Outlier("Test", 1);
    };
    C_Date("T3GUTT03",
21700, 2600)
    {
     color="Orange";
     Outlier("Test", 0.2);
    };
   };
   Boundary("Boundary Limit
6")
   {
    color="Red";
   };
   Phase("Zone 5 Scottish
(?) readvance")
   {
    C_Date("T3ALDO01",
20200, 3500)
    {
     color="Orange";
     Outlier("Test", 0.2);
    };
    C_Date("T3ALDO02",
27900, 4700)
    {
     Outlier();
     color="Orange";
    };
   };
   Boundary("Boundary Limit
7")
   {
    color="Red";
   };
   Phase("Zone 6 Galloway
Hills")
   {
    C_Date("GB-02", 12000,
1200)
    {
     color="Blue";
     Outlier();
    };
    C_Date("GB-03", 14800,
1200)
    {
     color="Blue";
     Outlier("Test", 0.2);
    };
    C_Date("GB-04", 15100,
900)
    {
     color="Blue";
     Outlier("Test", 0.2);
    };
    C_Date("GB-06", 14700,
1400)
    {
     Outlier("Test", 0.2);
     color="Blue";
    };
    C_Date("GT-01", 15100,
900)
    {
     color="Blue";
     Outlier("Test", 0.2);
    };
```

```
   C_Date("GT-2.1", 15500,
800)
   {
    color="Blue";
    Outlier("Test", 0.2);
   };
   C_Date("GT-2.2", 15300,
800)
   {
    color="Blue";
    Outlier("Test", 0.2);
   };
   C_Date("GT-03", 14000,
700)
   {
    color="Blue";
    Outlier("Test", 0.2);
   };
  };
  Boundary("Boundary Limit
8")
   {
    color="Red";
   };
  };
  C_Date("T3GUTT01",
27000, 3300)
  {
   Outlier();
   color="Orange";
  };
 };
```

BAYESIAN MODELLING CODE FOR RETREAT IN NORTHEAST IRELAND

```
 Options()
 {
  BCAD=FALSE;

Delta_R("LocalMarine",0,0);

Curve("Marine13","Marine1
3.14c");
 };
 Plot()
 {
  Outlier_Model("T3-
NIreland", T(5), U(0,4), t);
  Sequence("Retreat T3 n
Ireland")
  {
   Boundary("Retreat N
Ireland")
   {
    color="Red";
   };
   Phase("Kilkeel")
   {
    R_Date("Kilkeel steps1b",
17150, 160)
    {
     Outlier("Test", 0.05);
    };
    R_Date("Kilkeel steps1a",
17160, 130)
    {
     Outlier("Test", 0.05);
    };
    R_Date("Kilkeel steps2",
17040, 70)
    {
     Outlier("Test", 0.05);
    };
    R_Date("Kilkeel steps3",
16940, 70)
    {
     Outlier("Test", 0.05);
    };
    R_Date("Kilkeel steps4",
17370, 190)
    {
     Outlier("Test", 0.05);
    };
   };
   Boundary("Ice margins
on-land NE Ireland")
   {
    color="Red";
   };
   Phase("Cooley Pt - Port:
ice free episode")
   {
    R_Date("Cooley
AA17693", 15420, 110)
    {
     Outlier("Test", 0.05);
    };
    R_Date("Cooley
AA17694", 15790, 110)
    {
     Outlier("Test", 0.05);
    };
    R_Date("Cooley
AA17695", 15800, 140)
    {
     Outlier("Test", 0.05);
    };
    R_Date("Port AA68976",
15590, 85)
    {
     Outlier("Test", 0.05);
    };
    R_Date("Port AA68975",
15700, 90)
    {
     Outlier("Test", 0.05);
    };
    R_Date("Port
CAMS105063", 15850, 45)
    {
     Outlier("Test", 0.05);
    };
    R_Date("Port
CAMS105064", 16440, 550)
    {
     Outlier("Test", 0.75);
    };
   };
   Boundary("Clogher Head
readvance")
   {
    color="Red";
   };
   Phase("Cranfield Point")
   {
    R_Date("Cranfield
AA21819", 16005, 140)
    {
     Outlier("Test", 0.75);
    };
    R_Date("Cranfield
AA21818", 15105, 130)
    {
     Outlier("Test", 0.05);
    };
   };
   Boundary("Ice free
Cranfield Point")
   {
    color="Red";
   };
   Phase("Linns-Rathcor")
   {
    R_Date("Rathcor
AA56701", 14650, 130)
    {
     Outlier("Test", 0.05);
    };
    R_Date("Linns AA56700",
14557, 69)
    {
     Outlier("Test", 0.05);
    };
   };
   Boundary("Killard point
readvance")
   {
    color="Red";
   };
   Phase("Killard")
```

```
 {
  R_Date("Killard Point2", 13785, 115)
  {
   Outlier("Test", 0.05);
  };
  R_Date("Killard Point1", 13995, 105)
  {
   Outlier("Test", 0.05);
  };
 };
  Boundary("Killard Point retreat")
  {
   color="Red";
  };
  Phase("Rough Island")
  {
   R_Date("Rough AA21822", 12740, 95)
   {
    Outlier("Test", 0.05);
   };
   R_Date("Rough AA68680", 13525, 70)
   {
    Outlier("Test", 0.05);
   };
  };
  Boundary("End")
  {
   color="Red";
  };
 };
};
```

D_e VALUES DETERMINED FOR OSL DATING

Table S1. D_e values from OSL dating of sample T3TURK01.

D_e (Gy)	D_e Uncertainty (Gy)	Net T_n signal in response to 10.6 Gy (cts/0.1 s)
4.56	4.09	78
35.11	5.11	259
35.75	6.69	3954
124.68	15.54	359
38.01	9.95	72
7.81	3.41	61
18.20	4.26	107
13.37	3.58	67
48.08	7.13	351
28.55	2.94	371
25.24	2.18	1829
97.35	10.48	1598
36.18	3.22	805
16.78	2.42	292
72.18	17.55	100
7.55	3.61	97
32.41	20.12	70
28.11	3.48	1231
83.25	31.69	3754
46.40	9.92	75
11.72	5.98	80
32.50	3.82	282
78.59	19.87	125
23.20	3.57	288

31.44	2.10	1328
27.61	5.27	91
39.77	10.21	874
2.89	6.58	58
23.91	6.01	59
45.17	25.06	81
31.64	4.85	211
131.92	20.34	1574
34.03	4.92	509
17.33	3.22	389
33.97	3.87	249
49.42	11.96	124
24.70	7.01	63
22.68	3.44	230
34.77	2.54	678
32.15	7.08	66
61.48	6.36	563
40.42	6.75	240
13.83	3.38	189
3.82	2.53	119
12.29	3.39	104
50.34	9.94	110
36.71	4.32	256
38.14	6.35	195
37.76	14.31	77
25.89	2.12	657
8.98	22.50	81

Table S2. D_e values from OSL dating of sample T3BALH01.

D_e (Gy)	**D_e Uncertainty (Gy)**	**Net T_n signal in response to 12.9 Gy (cts/0.1 s)**
187.98	14.25	2998
100.13	18.92	77
73.03	14.64	129
24.51	6.00	69
8.82	2.63	122

12.88	5.88	65
9.79	3.72	54
67.12	12.93	113
67.31	11.84	106
148.27	48.01	157
67.74	20.04	62
57.27	11.83	72
31.12	7.47	320
99.20	28.96	613
29.58	4.93	124
33.67	9.47	138
95.38	30.85	197
113.02	6.93	1771
71.23	20.40	60
22.30	6.13	338
100.47	25.08	71
21.99	6.55	78
58.30	4.34	1096
112.52	25.35	1770
148.57	34.25	87
27.74	10.46	198
29.93	4.73	133
19.56	2.70	177
75.80	5.65	2267
54.34	5.33	1510
65.37	27.58	52
163.20	22.41	924
52.66	16.84	243
47.86	15.86	66
60.80	14.42	61
30.66	3.80	195
31.89	7.36	389

29.28	10.47	73
25.23	5.60	68
75.47	10.90	159
74.77	9.39	487
137.21	13.99	490
99.00	16.90	238
81.39	5.56	1869
15.23	1.94	273
76.30	11.88	127
16.59	2.09	837
183.92	18.78	448
32.63	5.10	107

Table S3. D_e values from OSL dating of sample T3BALH02.

D_e (Gy)	**D_e Uncertainty (Gy)**	**Net T_n signal in response to 12.9 Gy (cts/0.1 s)**
11.61	20.94	67
32.29	8.48	65
48.99	14.74	38
115.56	13.83	192
33.28	6.85	111
63.08	8.78	2503
25.53	2.54	568
53.73	14.12	58
110.53	32.85	100
115.40	8.30	1145
73.94	11.39	107
92.90	25.18	99
41.98	14.75	103
6.58	20.74	127
77.48	9.79	286
70.72	6.93	417
40.10	6.08	130

23.20	6.19	125
14.50	5.46	76
54.57	19.98	84
23.13	6.78	64
135.42	33.39	2714
101.10	14.29	185
116.50	113.46	79
42.00	10.01	59
43.89	8.79	95
105.29	21.15	205
26.03	3.64	162
39.70	3.78	377
48.47	9.56	244
154.56	163.20	46
35.13	5.96	81
170.23	18.91	287
135.15	42.70	49
17.75	21.83	107
89.83	12.35	1015
88.15	49.48	41
60.97	9.47	375
58.05	19.08	83
83.99	23.93	99
158.29	27.15	76
20.70	4.50	107
56.95	17.43	49
63.55	11.80	238
33.96	5.26	218
82.77	4.60	1356
41.42	23.06	115
33.88	8.55	94
23.71	1.39	7739

63.76	8.69	212
173.07	23.50	120
78.59	10.69	3131
67.09	17.31	90
148.42	13.86	874
33.64	6.66	98
80.62	17.22	46
40.50	10.02	75
84.32	8.42	321
21.63	3.71	110
37.63	9.76	55
122.40	22.67	531
43.97	9.90	141
81.57	6.21	781
132.02	83.84	39
64.31	10.99	132

Table S4. D_e values from OSL dating of sample T3ORIS01.

D_e (Gy)	**D_e Uncertainty (Gy)**	**Net T_n signal in response to 10.6 Gy (cts/0.1 s)**
141.05	21.45	148
80.24	40.18	130
0.66	1.50	159
0.01	1.51	190
10.96	5.60	63
53.62	8.45	1069
48.81	10.32	77
69.59	12.99	116
58.33	30.66	52
17.94	6.34	69
9.31	4.95	68

30.01	4.37	817
91.35	37.53	943
62.18	17.12	75
36.92	3.78	278
38.28	7.76	380
56.83	8.10	169
70.78	21.35	75
32.73	11.99	76
40.56	8.86	122
142.61	35.26	669
83.75	24.85	658
52.90	17.03	270
29.60	7.29	414
38.82	2.84	3463
36.56	7.11	258
68.63	17.85	199
75.38	21.53	105
81.66	8.34	1770
62.25	8.26	288
41.47	8.03	144
31.59	4.02	201
61.01	15.50	889
62.21	18.41	73
98.07	7.73	462
15.14	4.09	74
33.29	6.94	121
131.02	14.33	347

42.41	2.44	1414
55.79	6.28	418
40.45	5.38	320
57.53	11.79	102
38.35	6.57	258
135.88	27.96	235
70.99	14.29	120
85.04	18.52	78
67.33	9.25	284
38.21	2.71	649
69.03	14.55	1157
42.11	6.16	190
33.37	9.54	65
44.38	2.73	3225
130.60	33.82	205
50.70	46.35	205
100.64	15.33	204
72.45	12.20	85
24.27	12.02	50
68.14	9.45	529
82.20	44.28	66
44.09	8.12	86
90.79	31.49	62
34.60	5.95	192
96.67	22.56	112
78.31	18.13	110
55.42	13.50	98

26.55	19.70	56
21.65	4.00	81
92.75	23.16	84
26.56	9.62	60
56.50	5.72	384
94.06	13.33	544
37.60	8.35	321
24.85	9.85	51
97.60	18.81	156
132.22	13.32	268
139.89	19.17	111
102.09	22.59	81
24.84	6.87	51
103.17	27.73	56
58.97	9.13	137
129.26	15.95	313
45.80	5.88	142
37.23	11.13	103
37.80	7.15	200
108.27	81.65	188
70.89	15.31	247
30.25	4.47	184
30.16	23.28	49
54.38	31.15	74
45.32	4.20	819
45.38	7.84	103
89.42	12.04	178

74.02	6.00	554
9.42	5.52	31

Table S5. D_e values from OSL dating of sample T3DOGM01.

D_e (Gy)	**D_e Uncertainty (Gy)**	**Net T_n signal in response to 12.9 Gy (cts/0.1 s)**
51.32	3.63	1393
37.25	8.79	62
23.71	3.01	261
34.32	10.55	40
84.35	18.35	66
45.06	7.98	161
43.87	35.20	123
99.13	18.01	2331
128.35	33.40	286
52.75	7.15	142
37.66	15.16	86
21.54	2.32	462
78.62	16.89	114
51.61	11.64	68
52.65	9.00	242
67.03	9.28	110
61.27	6.28	791
55.10	18.89	37
30.28	3.99	162
62.35	8.01	295
50.41	79.18	53
16.46	6.66	53

20.65	3.40	103
43.63	17.59	79
58.12	6.01	2112
35.95	8.21	395
35.48	4.36	208
41.79	2.11	6054
48.62	13.67	65
62.54	14.84	97
53.15	12.81	50
35.13	7.72	86
42.54	20.38	40
112.57	22.98	56
95.21	68.82	139
87.37	24.27	37
33.93	3.77	266
10.63	7.83	129
62.96	15.22	61
40.88	3.34	612
127.29	8.74	755
42.37	8.05	106
18.39	11.87	56
27.31	3.06	318
26.65	19.75	54
35.28	5.61	117
77.92	7.76	284
52.79	12.43	71
151.78	37.00	56

30.30	1.94	5672
30.23	24.19	128
34.50	4.13	239
41.75	16.46	82
23.34	12.93	55
34.28	9.02	64
29.84	8.25	47
32.38	4.12	305
72.09	53.80	82
56.23	9.04	329
106.45	19.01	483
39.87	7.21	171
28.21	16.77	44
122.79	23.18	111
27.65	6.75	54
32.82	10.32	186
28.74	3.92	156
59.32	18.96	49
21.32	5.44	66
31.40	5.46	196
47.90	10.70	53
63.24	13.72	211
64.08	17.29	89
64.22	17.83	210
54.34	9.78	120
96.12	77.00	73
82.65	18.89	88

43.92	14.25	95

Table S6. D_e values from OSL dating of sample T3JURB01.

D_e (Gy)	D_e Uncertainty (Gy)	Net T_n signal in response to 10.6 Gy (cts/0.1 s)
73.05	8.76	127
23.67	5.90	80
31.11	9.10	61
54.10	11.85	87
45.41	19.28	126
25.99	1.63	1604
91.43	19.89	134
45.16	18.28	77
45.08	7.85	163
79.42	16.72	92
33.57	5.51	189
48.49	10.23	124
26.16	13.76	104
57.95	18.35	92
86.91	12.25	22564
101.59	8.28	585
30.53	11.21	50
59.59	31.28	92
43.49	15.12	67
134.50	28.21	103
86.79	9.59	893
34.63	5.21	429
58.10	12.86	103
101.69	20.54	137

151.35	27.46	86
42.99	13.41	108
57.68	7.06	446
60.80	7.14	375
45.20	10.76	506
85.60	20.39	119
32.58	6.16	213
98.84	8.68	1841
73.13	8.07	362
16.77	2.25	262
62.12	9.45	245
37.33	4.30	313
102.06	31.27	68
34.90	4.58	559
70.18	22.93	121
118.70	19.16	101
133.84	14.28	604
21.26	1.26	1621
25.76	4.14	530
70.67	6.92	6430
34.88	6.12	106
82.31	13.96	279
39.13	7.48	309
51.17	55.59	97
23.77	5.90	71
97.20	33.76	135
88.08	49.17	62

75.79	9.71	259
39.33	167.65	44
98.13	25.25	53
14.50	2.52	221
26.79	5.62	201
38.82	2.69	1753
44.08	5.58	166
38.01	14.20	60
13.04	5.68	58
43.63	9.21	76
28.72	14.36	51
29.22	6.11	109
23.26	3.99	152
19.65	2.22	332
20.18	2.69	342
33.07	4.29	186
19.16	8.06	115
33.49	6.79	104
56.27	14.52	60
94.05	19.72	117
83.34	12.75	171
43.44	6.78	945
40.36	6.32	587
79.43	28.39	780
29.57	6.42	76
23.37	6.79	91
29.36	4.63	214

62.29	12.19	81
32.71	8.02	68
8.76	3.31	117
9.78	5.25	43
21.85	2.62	246
47.73	6.37	275
45.70	12.19	262
29.26	3.15	648
47.00	5.59	3664
46.44	16.94	221
30.39	8.35	77
18.08	4.24	145
45.51	18.66	175
32.89	9.05	46
41.57	4.73	210
62.39	8.57	819
34.42	19.44	154
43.07	2.18	9552
35.01	10.60	40
51.84	24.80	65
30.00	4.85	284
36.74	10.02	46
79.83	21.57	60
41.39	4.33	847
20.42	2.51	222
58.20	16.91	61
70.41	6.04	902

Table S7. D_e values from OSL dating of sample T3JURB02.

D_e (Gy)	D_e Uncertainty (Gy)	Net T_n signal in response to 10.6 Gy (cts/0.1 s)
37.66	7.69	246
46.91	6.04	277
85.75	30.60	277
8.21	3.41	69
107.53	37.69	106
47.66	9.42	282
22.94	6.40	79
55.04	9.11	140
107.55	9.58	876
156.10	41.10	379
88.91	96.72	123
46.16	7.99	344
68.04	4.30	912
71.36	13.22	581
64.65	8.31	133
61.29	14.47	116
110.85	12.27	749
27.71	3.18	259
84.36	9.02	3313
65.02	37.42	249
41.07	10.15	95
38.63	4.81	520
26.01	1.69	1014
62.42	5.73	1443
50.55	16.66	283

26.43	12.01	88
48.67	8.16	166
124.07	7.82	1778
88.97	5.98	4186
85.46	12.43	224
25.34	2.12	925
52.79	5.80	353
42.10	2.47	1139
72.83	9.46	351
36.19	17.90	312
40.86	6.34	288
88.24	9.08	428
48.42	4.88	484
21.00	7.37	73
100.45	24.80	304
68.51	3.78	4122
20.88	6.89	125
38.57	22.04	125
76.51	70.72	134
44.26	2.24	3369
28.80	5.17	131
29.94	9.50	74
76.24	25.58	84
60.02	3.32	1714
39.73	3.57	470
53.46	7.50	156
115.27	9.49	8317

30.63	7.81	78
36.49	7.31	114
30.27	3.84	314
97.44	6.19	1590
58.11	11.54	135
75.11	19.88	114
77.11	31.21	1219
55.73	5.69	478
22.78	4.07	421
20.48	3.17	126
48.81	9.00	307
50.48	23.41	100
70.74	10.07	335
26.85	14.03	188
33.87	6.83	125
36.40	9.42	213
23.07	5.30	67
89.93	22.32	10618
26.63	5.11	172
73.32	6.72	318
29.77	6.25	219
45.60	33.38	1174
83.81	11.42	206
36.81	3.71	459
59.23	12.62	139
28.09	3.54	184
59.04	3.97	60304

26.98	4.47	192
71.51	20.99	150
34.44	3.22	12389
42.87	5.20	186

Table S8. D_e values from OSL dating of sample T3GUTT01.

D_e (Gy)	**D_e Uncertainty (Gy)**	**Net T_n signal in response to 13.0 Gy (cts/0.1 s)**
110.93	13.61	439
67.53	6.86	264
26.13	7.31	60
199.15	22.16	202
21.68	4.10	112
17.04	4.50	68
159.82	20.19	143
74.31	24.20	39
166.36	47.00	60
53.50	12.97	105
122.87	22.62	82
82.40	24.55	45
171.83	62.33	53
153.23	40.27	82
100.09	27.12	130
110.83	17.68	64
201.41	34.21	171
213.10	33.72	105
116.22	20.56	104
149.24	20.51	178
86.68	25.45	62

120.19	28.74	59
56.48	15.94	44
52.73	7.82	170
107.87	31.02	94
107.23	32.20	136
104.01	19.91	82
101.53	29.84	51
132.80	32.17	54
84.52	27.08	155
142.14	33.72	55
49.70	9.01	107
87.93	16.02	75
133.90	41.60	47
52.64	14.17	53
180.86	30.79	87
167.51	18.61	236
45.88	11.53	50
27.24	9.53	48
15.86	5.40	53
41.49	25.92	65
197.77	45.27	123
29.34	13.73	40
101.51	16.45	409
129.73	14.13	210
77.83	39.25	331
107.02	82.09	123
160.77	133.44	71

90.89	24.75	83
51.23	7.71	622
40.24	7.31	130
87.88	30.29	52
57.53	20.53	88
88.71	12.89	97
125.02	9.31	777
83.46	27.48	53
137.31	67.27	115
18.68	3.26	161
88.77	17.29	98
70.56	12.10	53
37.17	11.06	200
112.46	41.81	95
46.95	8.67	118
51.63	20.52	60
142.43	26.22	95
16.13	3.94	61
136.32	33.85	63
44.30	16.19	67
129.55	24.90	226
135.51	35.39	110
127.09	27.78	65
168.48	33.55	67
136.34	27.19	125
123.93	27.57	148
103.04	18.85	111

93.19	21.50	73
155.28	15.29	408
58.29	9.62	128
147.23	20.28	140
74.18	20.58	74
113.47	20.60	156
131.97	20.47	89
26.09	1.96	2076
63.49	33.00	63
154.21	34.94	482
115.30	33.58	53
78.13	25.46	49
114.73	33.22	524
39.49	17.98	137
84.83	18.66	110
85.87	25.27	68
36.56	8.52	137
89.31	28.13	113
116.83	9.46	1143
76.36	15.72	117
91.48	27.63	95
75.89	8.11	492
129.13	47.82	578
73.57	29.02	147
63.97	15.49	137
81.22	7.07	669
75.71	16.70	87

129.47	37.55	101
132.34	54.33	136
89.15	34.48	463

Table S9. D_e values from OSL dating of sample T3GUTT03.

D_e (Gy)	**D_e Uncertainty (Gy)**	**Net T_n signal in response to 12.6 Gy (cts/0.1 s)**
77.80	14.26	152
129.67	13.88	159
119.53	16.53	69
147.27	56.91	45
52.07	7.49	563
74.79	14.77	68
35.18	8.36	181
83.91	20.24	79
37.91	4.69	258
59.77	19.57	178
65.96	11.61	143
29.60	13.89	91
132.79	45.75	162
68.59	17.36	104
45.28	8.90	81
70.59	20.88	60
91.44	20.87	62
23.37	8.77	65
57.17	15.42	92
104.32	17.86	122
127.90	19.30	62
51.34	8.37	182
116.46	5.12	5786
30.95	10.59	141
155.76	34.88	72

147.56	50.63	54
57.45	23.40	65
75.22	5.64	451
32.30	10.59	53
71.25	18.98	191
45.07	5.63	405
133.25	27.31	48
73.93	18.27	48
59.34	36.67	263
57.08	15.52	93
8.07	8.15	59
80.91	12.26	164
118.30	25.28	1428
72.32	17.13	162
77.13	14.53	57
82.01	6.67	971
68.75	17.46	64
133.31	18.41	113
81.89	69.06	169
122.88	24.54	71
39.06	5.36	201
65.28	9.16	179
52.76	30.47	136
136.08	26.83	71
35.78	6.01	170
130.68	62.83	48
73.98	11.65	168
39.08	4.36	425
96.96	16.37	59
44.76	19.76	128
52.81	13.03	75
70.02	11.85	52

153.56	25.88	46
19.14	4.12	125
58.16	14.84	69
32.78	5.51	106
57.06	28.35	54
120.24	49.01	141
50.15	11.79	101
39.60	12.59	42
75.16	26.37	58
86.56	14.00	132
157.28	26.70	88
103.95	16.56	455
31.61	7.35	89
144.39	20.00	207
80.96	22.79	44
110.96	17.76	54
126.43	39.29	48
116.37	28.52	49
155.00	36.82	118
64.67	7.51	520

Table S10. D_e values from OSL dating of sample T3ALDO01.

D_e (Gy)	**D_e Uncertainty (Gy)**	**Net T_n signal in response to 12.9 Gy (cts/0.1 s)**
89.54	65.50	44
52.95	14.07	129
149.96	40.70	50
17.88	5.01	49
92.05	38.66	141
45.78	14.30	48
205.99	23.26	370
197.11	88.52	72
80.57	20.19	68

123.72	26.30	70
140.75	33.37	65
168.06	112.77	155
40.36	10.34	48
121.99	18.21	218
63.44	15.76	149
128.38	29.64	81
133.43	107.37	69
26.70	6.26	93
186.71	37.31	713
190.99	47.34	45
79.08	19.36	64
175.55	30.69	109
125.97	15.95	265
150.58	28.99	114
137.19	92.72	73
71.78	19.28	61
87.91	34.97	33
15.71	3.44	108
148.12	85.66	47
104.89	14.20	139
141.52	22.66	172
162.23	23.77	92
151.39	69.09	50
17.18	4.26	101
16.30	7.40	62
94.20	39.82	91
84.68	30.89	52
96.91	29.41	51
80.51	15.30	154
48.90	11.63	60
111.86	22.47	56

51.90	10.37	69
197.26	23.24	445
140.05	22.57	177
65.41	26.39	61
76.76	27.54	42
174.54	32.90	60
105.63	7.60	217
75.05	17.13	100
86.33	20.33	48
109.73	24.99	62
64.74	19.51	46
47.26	16.69	80
127.51	31.90	58
60.76	14.38	56
114.94	29.96	73

Table S11. D_e values from OSL dating of sample T3ALDO02.

D_e (Gy)	**D_e Uncertainty (Gy)**	**Net T_n signal in response to 12.9 Gy (cts/0.1 s)**
149.06	35.74	48
106.57	21.55	98
119.93	30.94	47
133.63	32.46	38
172.01	72.25	67
53.13	10.26	67
169.46	26.08	114
107.74	62.15	58
113.63	32.79	70
113.31	18.37	863
16.45	4.39	153
70.61	12.47	105
113.08	13.71	1056
179.49	97.68	76

106.60	13.97	1294
56.22	11.92	54
92.24	22.42	113
179.38	25.19	238
102.27	22.24	59
180.07	68.11	52
78.70	20.92	82
168.14	44.15	130
112.33	37.88	127
110.64	21.58	84
227.76	103.37	111
137.13	39.61	50
191.80	38.19	101
56.90	13.80	50
15.42	2.08	243
39.05	11.65	47
26.33	39.52	44
93.91	20.38	46
87.91	11.27	250
67.88	12.66	216
183.49	35.87	51
139.81	38.93	187
278.75	112.63	72
101.17	34.83	59
65.57	7.19	340
65.92	20.42	45
17.33	5.25	84
101.65	31.65	50
89.28	18.62	86
74.77	15.80	81
40.06	14.24	48
192.50	75.34	60

116.62	18.50	84
183.06	81.81	243
203.92	32.47	84
157.24	22.44	86
22.71	8.98	42
116.59	80.79	57
209.58	26.15	362
92.32	40.58	60
20.37	11.29	54
132.75	25.18	71
131.21	52.66	52
74.86	16.07	70
138.40	155.09	94
153.62	27.84	58
107.79	25.48	46
172.87	31.32	89
27.92	9.52	77
190.61	39.71	48